Taylor & Francis
Taylor & Francis Group

MSC-mediated mitochondrial transfer promotes metabolic reprograming in endothelial cells and vascular regeneration in ARDS

Jinlong Wang[a,b]*, Shanshan Meng[a]*, Yixuan Chen[a], Haofei Wang[a], Wenhan Hu[a], Shuai Liu[a], Lili Huang[a], Jingyuan Xu[a], Qing Li[a], Xiaojing Wu[a], Wei Huang[a] and Yingzi Huang[a]

[a]Jiangsu Provincial Key Laboratory of Critical Care Medicine, Department of Critical Care Medicine, Zhongda Hospital, School of Medicine, Southeast University, Nanjing, People's Republic of China; [b]Department of Critical Care Medicine, The First Affiliated Hospital of Anhui Medical University, Hefei, People's Republic of China

ABSTRACT

Background: Mesenchymal stem cells (MSCs) are a potential therapy for acute respiratory distress syndrome (ARDS), but their mechanisms in repairing mitochondrial damage in ARDS endothelial cells remain unclear.
Methods: We first examined MSCs' mitochondrial transfer ability and mechanisms to mouse pulmonary microvascular endothelial cells (MPMECs) in ARDS. Then, we investigated how MSC-mediated mitochondrial transfer affects the repair of endothelial damage. Finally, we elucidated the mechanisms by which MSC-mediated mitochondrial transfer promotes vascular regeneration.
Results: Compared to mitochondrial-damaged MSCs, normal MSCs showed a significantly higher mitochondrial transfer rate to MPMECs, with increases of 41.68% in vitro ($P < 0.0001$) and 10.50% in vivo ($P = 0.0005$). Furthermore, MSC-mediated mitochondrial transfer significantly reduced reactive oxygen species ($P < 0.05$) and promoted proliferation ($P < 0.0001$) in MPMECs. Finally, MSC-mediated mitochondrial transfer significantly increased the activity of the tricarboxylic acid (TCA) cycle (MD of CS mRNA: 23.76, $P = 0.032$), and further enhanced fatty acid synthesis (MD of FAS mRNA: 6.67, $P = 0.0001$), leading to a 6.7-fold increase in vascular endothelial growth factor release from MPMECs and promoted vascular regeneration in ARDS.
Conclusion: MSC-mediated mitochondrial transfer to MPMECs activates the TCA cycle and fatty acid synthesis, promoting endothelial proliferation and pro-angiogenic factor release, thereby enhancing vascular regeneration in ARDS.

Introduction

Acute Respiratory Distress Syndrome (ARDS) represents a significant challenge in the field of critical care medicine, characterized by a high incidence and mortality rate, imposing a substantial burden on patients and healthcare systems worldwide. According to global epidemiological data, the incidence of ARDS is showing an increasing trend year by year, with millions of new cases emerging globally each year, and the mortality rate often exceeds 30% [1,2]. Epidemiological data from China indicates that the hospital mortality rate of ARDS is 34%, and even higher for severe ARDS, reaching up to 60% [3]. Over the past two decades, clinical treatment progress for ARDS has remained at the level of organ support, such as lung-protective ventilation strategies and prone positioning ventilation, lacking effective treatment targeting the pathogenesis and pathological changes of ARDS [4].

Mesenchymal Stem Cells (MSCs), characterized by their pluripotency, self-renewal, and immunomodulatory capabilities, have emerged as a promising therapeutic strategy for ARDS. Firstly, Recent studies have highlighted the role of MSCs in modulating both innate and adaptive immune responses in ARDS, leading to a reduction in lung injury attributable to excessive inflammation [5,6]. Secondly, MSCs have been shown to enhance pathogen clearance and mitigate both direct and inflammatory damages [7]. Thirdly, MSCs facilitate the repair of alveolar epithelial and pulmonary endothelial cells, thereby restoring the integrity of the alveolar-capillary barrier and improving pulmonary fluid clearance [8]. Lastly, the potential of MSCs to differentiate into damaged lung tissues positions MSCs as a pivotal agent in promoting lung repair in ARDS [9]. However, the mechanisms by which MSCs repair ARDS lung injury have not yet been fully elucidated.

Mitochondrial damage plays a crucial role in the pathogenesis and progression of ARDS [10–12]. Specifically, mitochondrial damage can lead to disturbances in cellular energy metabolism, weakening the cell's adaptability to stress and exacerbating the progression of ARDS [13]. Changes in mitochondrial membrane permeability trigger the release of mitochondrial DNA, provoking an intensified inflammatory response by the immune system [14]. Alterations in the protein channels of the mitochondrial membrane directly result in apoptosis and necrosis of endothelial and epithelial cells. Additionally, mitochondria are involved in oxygen sensing and cell signaling, mitochondrial damage can lead to dysregulation of cellular signaling pathways [15].

Mitochondrial transfer refers to the process where mitochondria are transported from one cell to another. This phenomenon was first observed in a 2006 study, which showed that ρ0 cells, lacking mitochondrial DNA, could restore mitochondrial function by receiving mitochondria transferred from neighboring cells [16]. Building on this, the study by An et al. further confirmed in vivo that mtDNA is horizontally transferred from host cells in the tumor microenvironment to tumor cells with impaired respiratory function [17]. Mitochondrial transfer can occur between cells through various mechanisms, including transfer via extracellular vesicles, establishment of tunneling nanotubes (TNTs), and release of wandering mitochondria by donor cells for capture by recipient cells [18,19]. Upon receiving healthy mitochondria, the recipient cells experience a restoration of impaired mitochondrial function, stabilizing their energy metabolism and maintaining the functionality of various organs under disease conditions [18].

MSCs can repair mitochondrial damage in ARDS through mitochondrial transfer. Since Islam et al. first discovered that MSCs could transfer mitochondria to ARDS alveolar epithelial cells, restoring their aerobic metabolism [20], mitochondrial transfer has gained increasing attention in the field of ARDS lung injury repair. Recent studies have shown that MSCs can transfer mitochondria to alveolar macrophages in ARDS, enhancing their phagocytic ability and increasing the efficiency of pathogen clearance [21,22]. Additionally, MSCs can transfer mitochondria to T cells, increasing the proportion of regulatory T cells and exerting anti-inflammatory effects [23,24]. However, it remains unclear whether MSCs can transfer mitochondria to ARDS pulmonary endothelial cells and exert a reparative effect. This study aims to explore whether MSCs transfer mitochondria to ARDS pulmonary endothelial cells and to elucidate the potential role and mechanism of mitochondrial transfer in promoting the repair of ARDS endothelial injury.

Materials and methods

Establishment of animal and cell models

Husbandry of C57BL/6J mice

Male C57BL/6J mice, aged 5–8 weeks, were procured from GemPharmatech (Nanjing, China). Upon arrival, the mice were housed in a specific pathogen-free (SPF) environment, where the ambient temperature was maintained at $22 \pm 2°C$ with a relative humidity of $50 \pm 10\%$, adhering to a 12-hour light/dark cycle. The mice were kept in standard ventilated cages, with 3–5 mice per cage. Access to food and water was provided ad libitum. The Animal Experimental Ethics Committee of Southeast University approved these experiments (Approval number 20200226001).

Establishment of the ARDS mouse model

ARDS mouse model was established using chemical induction method. The mice were first anesthetized with 2–3% isoflurane inhalation. Subsequently, tracheal intubation was performed, followed by the intratracheal injection of 5 mg/kg body weight of LPS (Beyotime, Shanghai, China) to establish the ARDS model. After the establishment of the model, the mice were returned to clean cages for recovery.

Intravenous injection of MSCs in mice

MSCs were administered to the experimental mice via tail vein injection. C57BL/6J mouse bone marrow-derived MSCs were purchased from OriCell, Suzhou, China. The experimental mice were fasted a day before the MSCs injection, while ensuring an adequate supply of water. After 4 hours of ARDS mouse modeling, the mice were secured on a specialized tail vein injection stand. MSCs were diluted in sterile saline to a concentration of 1×10^6 cells/200 μL and then slowly injected into the mouse tail vein. After the injection, the mice were returned to cages for recovery.

Culture, passaging, and cryopreservation of MSCs

Bone marrow-derived MSCs from C57BL/6J mice were expanded in vitro. The culture medium consisted of DMEM/F-12 (Gibco, Waltham, USA), 10% fetal bovine serum (Gibco, Waltham, USA), and 1% penicillin–streptomycin (Gibco, Waltham, USA). Cells were cultured in a humidified incubator at 37°C with 5%CO_2. When cells reached 80% to 90% confluency, passaging was performed.

For passaging, cells were first washed twice with PBS (Procell, Wuhan, China) and then treated with 1 mL of 0.25% trypsin-EDTA solution (Gibco, Waltham, USA) in a 25T flask. Cells were incubated at 37°C for 1–2 minutes until detachment from the flask bottom. Immediately, an equal volume of complete culture medium was added to neutralize trypsin activity. The cell suspension was transferred to a 15 mL centrifuge tube and centrifuged at 300×g for 5 minutes. The supernatant was discarded, and the cells were resuspended in fresh culture medium and seeded into new flasks for continued cultivation.

When MSCs reached the appropriate passage number for cryopreservation, they were first collected following the passaging steps. Then, Cells were resuspended at a concentration of 1×10^6 cells/mL in cryopreservation solution (NCM Biotech, Suzhou, China). The cell suspension was aliquoted into pre-chilled cryovials, which were then placed in a cryogenic box in a −80°C freezer overnight before transferring to liquid nitrogen for long-term storage.

Construction of Miro1 knockdown MSCs

MSCs were infected with the lentiviral vector GV654 (hU6-MCS-Ubiquitin-mCherry- IRES-Neomycin), purchased from GeneChem, Shanghai, China. For infection, MSCs were seeded at a density of 1×10^5 cells per well in 6-well plates. The following day, MSCs were infected with either the target lentivirus or a negative control lentivirus for 16 h. After infection, the medium was replaced with complete growth medium, and stable Miro1 knockdown MSCs (Miro1-KD MSCs) or negative control MSCs (NC MSCs) were selected using geneticin. Knockdown efficiency of the obtained MSCs was evaluated by qRT-PCR and Western blot.

Culture, passaging, and cryopreservation of MPMECs

We used an immortalized mouse pulmonary microvascular endothelial cells (MPMECs), which was established and validated as described in previous studies [25]. The culture medium comprised of basic DMEM/F-12, 5% fetal bovine serum, 1% endothelial cell growth supplement (ScienCell, San Diego, USA), 1% penicillin–streptomycin, 90U/mL heparin (Sigma-Aldrich, Darmstadt, Germany), and 92 mg/L D-valine (Sigma-Aldrich, Darmstadt, Germany). Cells were

maintained in a humidified incubator at 37°C with 5%CO$_2$, with fresh medium replacement every 1–2 days. Passaging was performed when cells reached 70–80% confluence.

For passaging MPMECs, cells were first washed twice with PBS and then treated with 1 mL of 0.25% trypsin-EDTA solution diluted ten-fold in PBS. Cells were incubated at 37°C for 1–2 minutes until detachment from the flask bottom. Subsequently, an equal volume of culture medium containing FBS was added to neutralize trypsin. The cell suspension was transferred to a centrifuge tube and centrifuged at 300×g for 5 minutes. The supernatant was discarded, and the cells were resuspended in fresh culture medium and seeded into new flasks for continued cultivation.

For cryopreservation of MPMECs, cells were first collected following the passaging protocol. Cells were resuspended at a concentration of 1×10^6 cells/mL in cryopreservation solution. The cell suspension was aliquoted into pre-chilled cryovials. The vials were then placed in a cryogenic box in a −80°C freezer overnight before transferring to liquid nitrogen for long-term storage.

Mitochondrial damage induction with rotenone

Rotenone (MedChemExpress, Monmouth Junction, USA) was employed to induce mitochondrial damage, simulating conditions of mitochondrial dysfunction in ARDS. Cells intended for the experiment were cultured to an appropriate density at 37°C and 5%CO$_2$ prior to treatment. The rotenone powder was initially dissolved in dimethyl sulfoxide (DMSO) (MedChemExpress, Monmouth Junction, USA) to prepare a high-concentration stock solution (1 mM). For experimental use, this stock solution was subsequently diluted to a final concentration of 100 nM in the culture medium. The final concentration of DMSO in the culture medium was 0.01%. During treatment, the culture medium containing rotenone was directly added to the cell culture dishes. The cells were stimulated for 4 hours. After the treatment, the medium containing rotenone was removed, and the cells were washed with PBS, followed by replacement with fresh culture medium for subsequent experiments.

Method details

Flow cytometry analysis of mitochondrial transfer from MSCs to MPMECs

MSCs and MPMECs were cultured separately until reaching 70–80% confluency, and mitochondria in MSCs were labeled with MitoTracker Deep Red FM (Invitrogen, Waltham, USA). Briefly, MitoTracker Deep Red FM was dissolved in DMSO to make a 1 mM stock solution and then diluted with complete culture medium to a working concentration of 200 nM (2 μL of stock solution added to 10 mL of complete culture medium). The final concentration of DMSO in the working solution was 0.02%. The culture medium was removed from the flasks, replaced with pre-warmed working solution, and the cells were incubated for 30 minutes. Afterward, the cells were washed with PBS and fresh culture medium was added.

For co-culture experiments, 1×10^5 mitochondria-prelabeled MSCs were co-cultured with MPMECs for 24 hours. Post co-culture, the cells were treated with 0.25% trypsin-EDTA for digestion, then collected by centrifugation (300 g, 5 minutes) and washed with PBS. Prior to flow cytometry, CD31 antibody (BD Pharmingen, Franklin Lakes, USA) was used to label surface proteins of MPMECs. Dual labeling with MitoTracker Deep Red FM and CD31 antibody allowed for the distinction between the two cell types in flow cytometry and the detection of MSCs' mitochondria in MPMECs.

Flow cytometry analysis of mitochondrial transfer from MSCs to MPMECs in ARDS mouse model

MSCs were cultured to 70–80% confluence and labeled with MitoTracker Deep Red FM for mitochondrial tracking. Four hours after ARDS mouse modeling, mitochondria-labeled MSCs were administered via tail vein injection to the ARDS model mice. Twenty-four hours later, the mice were euthanized, and their lung tissues were rapidly harvested. Under sterile conditions, the lung tissues were subjected to mechanical and enzymatic digestion to prepare single-cell suspension, which was then collected by centrifugation (300 g, 5 minutes) and washed with PBS.

MPMECs were labeled using fluorescently-tagged CD31 antibody. Flow cytometry was employed to distinguish between endothelial and non-endothelial cells, and to detect the presence of MSCs' mitochondria within MPMECs.

Immunofluorescence staining of mouse lung tissue to detect mitochondrial transfer from MSCs to MPMECs in ARDS

MSCs were labeled with MitoTracker Deep Red FM. Four hours post-establishment of the ARDS mouse model, mitochondria labeled MSCs were injected into the ARDS model mice via tail vein. Twenty-four hours after ARDS modeling, the mice were euthanized, and lung tissues were extracted and immediately frozen at −80°C. Frozen sections were then prepared, slicing the lung tissues into 5 μm thick sections.

The lung tissue sections underwent immunofluorescence staining, with primary antibody incubation using a CD31 antibody (Abcam, Cambridge, UK) for labeling MPMEC surface markers. Excess primary antibody was washed off, followed by incubation with a secondary antibody, Alexa Fluor 488 (Abcam, Cambridge, UK). Finally, the sections were observed and imaged using a fluorescence microscope. The co-localization of MSCs' MitoTracker labeling (red) with MPMECs' CD31 labeling (green) was analyzed to determine whether MSC mitochondria were transferred to MPMECs.

Confocal microscopy observation of mitochondrial transfer and tunneling nanotubes between MSCs and MPMECs

MSCs were labeled using MitoTracker Deep Red FM and MPMECs were labeled with MitoTracker Green FM (Invitrogen, Waltham, USA). Briefly, MPMECs were cultured in confocal dishes to 50% confluency. MitoTracker Green FM was dissolved in DMSO to make a 1 mM stock solution and then diluted with complete culture medium to a working concentration of 100 nM (1 μL of stock solution added to 10 mL of complete culture medium). The final concentration of DMSO in the working solution was 0.01%. The culture medium was removed from the confocal dishes, replaced with pre-warmed working solution, and the cells were incubated for 30 minutes. Subsequently, the cells were washed with PBS and fresh culture medium was added. Mitochondria-labeled MSCs were then added to the confocal dishes containing MPMECs and co-cultured for 12 hours. Under the confocal microscope, the co-localization of MSCs' mitochondria (red fluorescence) and MPMECs' mitochondria

(green fluorescence) was observed, along with the morphology of tunneling nanotubes.

Fluorescence microscopy observation of mitochondrial transfer from MSCs to MPMECs in isolated culture

MPMECs' mitochondria were labeled with MitoTracker Deep Red FM, and MPMECs were cultured in the lower chamber of the Transwell system. MSCs' mitochondria were labeled with MitoTracker Green FM, and pre-labeled MSCs were seeded in the upper chamber of the Transwell system. After 24 hours of isolated culture, fluorescence microscopy was performed. The co-localization of red and green fluorescence within MPMECs confirmed the transfer of mitochondria from MSCs to MPMECs during isolated culture.

Preparation of single-cell suspension from mouse lung tissue

Mice were euthanized following full anesthesia, and the lungs were rapidly excised and placed in pre-cooled PBS. Under sterile conditions, the lung tissues were thoroughly washed in PBS to remove blood. The washed tissues were then transferred to a sterile cutting board, where they were minced into 1–2 mm pieces using surgical scissors and tweezers. These tissue pieces were transferred to a digestion buffer containing collagenase (Beyotime, Shanghai, China) and DNase (Beyotime, Shanghai, China), and incubated at 37°C with gentle shaking for 1–2 hours to dissociate the tissue and release individual cells.

Following digestion, the mixture was filtered through a 100 μm cell strainer to remove undigested tissue fragments. The collected cell suspension was then centrifuged (300×g for 5 minutes), and the supernatant was discarded. Subsequently, the cell suspension was treated with red blood cell lysis buffer (Beyotime, Shanghai, China) to eliminate red blood cells. After 5 minutes, the suspension was centrifuged again, the supernatant was discarded, and the cells were resuspended in PBS warmed to room temperature.

Western blot analysis

Total protein was extracted from the target cells or tissues, and the protein concentration was determined using a BCA Protein Assay Kit (Beyotime, Shanghai, China). The protein samples were then mixed with SDS loading buffer and boiled at 95°C for 10 minutes to denature the proteins. Subsequently, the samples (15 μg) were loaded onto an SDS-PAGE gel for electrophoretic separation. After electrophoresis, the proteins were transferred to a PVDF membrane, which was then blocked with 5% BSA solution to prevent non-specific binding, and incubated at room temperature for 1 hour. The membrane was then incubated overnight at 4°C with primary antibody.

The next day, the membrane was washed three times with TBS containing 0.1% Tween-20 for 10 minutes each to remove excess primary antibody. This was followed by incubation with the corresponding HRP-conjugated secondary antibody (Beyotime, Shanghai, China) at room temperature for 1–2 h. After the incubation with the secondary antibody, the membrane was washed again and then treated with chemiluminescent substrate to detect the protein signal. To ensure consistency in protein loading, the membrane was also probed with an antibody against the internal control protein β-actin (Beyotime, Shanghai, China).

Flow cytometry analysis of CFSE mean fluorescence intensity in MPMECs

Flow cytometry was utilized to detect mean fluorescence intensity (MFI) of CFSE in MPMECs to evaluate cell proliferation. Initially, MPMECs were cultured to 50% confluency, and CFSE (Invitrogen, Waltham, USA) was added to the culture at a concentration of 5 μM. The cells were then incubated at 37°C with 5% CO_2 for 15–20 minutes. After incubation, cells were washed with PBS and resupplied with complete culture medium. Subsequently, 1×10^5 MSCs were added to the MPMEC culture system, and after 24 hours of co-culture, the treated cells were collected, washed with PBS, labeled with CD31 antibody to mark MPMECs, and prepared for flow cytometry analysis. In the flow cytometer, appropriate lasers and detectors were set to differentiate MPMECs while measuring the MFI of CFSE in MPMECs. Data were analyzed using FlowJo software, and cell proliferation was assessed by calculating the MFI of CFSE.

Flow cytometry analysis of ROS mean fluorescence intensity in MPMECs

Flow cytometry was employed to assess the level of reactive oxygen species (ROS) in MPMECs. MPMECs were cultured to 50% confluency and subjected to cell treatments according to experimental groups, with the MSC-treated experimental group receiving 1×10^5 MSCs. After 24 hours of co-culture with MSCs, the cells were collected. A specific ROS assay kit (Elabscience, Houston, USA) was used to treat the cell samples. Briefly, the ROS probe DCFDA was used for ROS detection, dissolving DCFDA at 10 μM in serum-free culture medium, and incubating MPMECs with this solution for approximately 20–30 minutes at 37°C. After incubation, cells were washed with PBS to remove uninternalized or unreacted DCFDA. Subsequently, cells were labeled and distinguished as MPMECs using a CD31 antibody. Flow cytometry analysis was performed to analyze the fluorescence signal, detecting and assessing the MFI of ROS in CD31-positive cells.

Flow cytometry analysis of cell apoptosis in MPMECs

Flow cytometry was utilized to assess apoptosis in MPMECs. Prior to the experiment, MPMECs were cultured to an appropriate density and subjected to experimental treatments, with 1×10^5 MSCs added to the MSC-treated group. After cell treatment, an Annexin V/PI Apoptosis Detection Kit (Elabscience, Houston, USA) was used for labeling and analysis. Firstly, the treated cells were collected and washed with PBS to remove serum and dead cells from the culture medium. The cell concentration was adjusted to 1×10^6 cells/mL, and then cells were resuspended in staining buffer containing Annexin V-FITC and PI, gently mixed to avoid excessive agitation. The cells were incubated in the dark at room temperature for 15–20 minutes. Following staining, MPMECs were labeled with CD31, and then analyzed using flow cytometry.

Hematoxylin and eosin staining and lung injury scoring of mouse lung tissue

Mouse lung tissues were stained with Hematoxylin and Eosin (H&E) to assess the extent of lung injury. Firstly, after experimental treatment, mice were euthanized, and lung tissues were rapidly excised. The tissues were fixed in 4%

paraformaldehyde solution for at least 24 hours to preserve the integrity of the tissue structure. After fixation, the lung tissues underwent dehydration, clearing, and paraffin infiltration, followed by embedding in paraffin blocks. The paraffin-embedded lung tissues were sectioned into 4–5 μm thick slices using a microtome and placed on slides. The slides were then dried at 60°C for about 30 minutes to enhance adhesion to the slides. Subsequently, H&E staining was performed. The sections were deparaffinized, hydrated through a series of graded ethanol solutions, stained with hematoxylin for 3–5 minutes to color the nuclei, rinsed with running water, and stained with eosin for 1–2 minutes to color the cytoplasm and other tissue structures. The sections were then dehydrated in ascending ethanol series, cleared, and mounted. After staining, images were observed and captured using an optical microscope.

The pathological injury of lung tissue was scored using the Smith scoring method. Lung edema, alveolar and interstitial inflammation, alveolar and interstitial hemorrhage, atelectasis, and hyaline membrane formation were semi-quantitatively analyzed with a score ranging from 0 to 4; where no injury scored 0, lesion area <25% scored 1, 25–50% scored 2, 50–75% scored 3, and lesion filling the field of view scored 4. The total lung injury score was the sum of these items, with the average score calculated from 10 high-power fields per animal.

Quantitative real-Time PCR analysis

The quantitative Real-Time PCR (qRT-PCR) technique was employed to analyze the mRNA expression levels of specific genes.

Total RNA was extracted using an RNA extraction kit (Takara, Tokyo, Japan). The concentration and purity of the extracted RNA were determined using a spectrophotometer to ensure RNA quality.

cDNA synthesis was performed using a reverse transcription kit (Takara, Tokyo, Japan). First, genomic DNA was removed from the total RNA, with the following reaction conditions: 42°C for 5 minutes, followed by storage at 4°C. The reaction system was as follows:

Reagent	Volume
gDNA Eraser	0.5 μL
gDNA Eraser Buffer	1 μL
RNA	x μL (500 ng)
DEPC-treated water	Up to 5 μL

Subsequently, reverse transcription was performed under the conditions: 37°C for 15 minutes, 85°C for 5 seconds, and stored at 4°C. The reaction system was as follows:

Reagent	Volume
PrimeScript RT Enzyme	0.5 μL
PrimeScript Buffer	2 μL
RT Primer Mix	0.5 μL
RNA free of gDNA	5 μL
DEPC-treated water	Up to 10 μL

The primers were synthesized by Shanghai Shenggong Biological Engineering Co., Ltd., China. The sequences of the primers are as follows:

Gene name	Sequence, 5′–3′	
	Forward	Reverse
Ki67	ATCATTGACCGCTCCTTTAGGT	GCTCGCCTTGATGGTTCCT
Mfn1	CCTACTGCTCCTTCTAACCCA	AGGGACGCCAATCCTGTGA
Mfn2	AGAACTGGACCCGGTTACCA	CACTTCGCTGATACCCCTGA
Miro1	TGGGCAGCACTGATAGAATAGA	GCAAAGACCGTAGCACCAAAG
HGF	ATGTGGGGGACCAAACTTCTG	GGATGGCGACATGAAGCAG
VEGF	CTGCCGTCCGATTGAGACC	CCCCTCCTTGTACCACTGTC
ACC	ATGGGCGGAATGGTCTCTTTC	TGGGGACCTTGTCTTCATCAT
ACLY	ACCCTTTCACTGGGGATCACA	GACAGGGATCAGGATTTCCTTG
FAS	GGAGGTGGTGATAGCCGGTAT	TGGGTAATCCATAGAGCCCAG
CS	GGACAATTTTCCAACCAATCTGC	TCGGTTCATTCCCTCTGCATA
IDH	ATGCAAGGAGATGAAATGACACG	GCATCACGATTCTCTATGCCTAA
OGDH	GTTTCTTCAAACGTGGGGTTCT	GCATGATTCCAGGGGTCTCAAA
β-actin	GGCTGTATTCCCCTCCATCG	CCAGTTGGTAACAATGCCATGT

The qRT-PCR reaction was performed using a qRT-PCR kit (Takara, Tokyo, Japan). The reaction conditions were as follows: pre-denaturation at 95°C for 30 seconds, followed by 40 cycles of denaturation at 95°C for 10 seconds, and annealing/extension at 60°C for 30 seconds. The reaction system was as follows:

Reagent	Volume
SYBR green Premix	5 μL
Upstream Primer	0.2 μL
Downstream Primer	0.2 μL
DEPC-treated water	2.6 μL
cDNA	2 μL

The internal reference gene β-actin was used as a control. The expression level changes of the target genes were calculated using the relative quantification method ($2^{-\Delta\Delta Ct}$ method).

Enzyme-Linked immunosorbent assay

Enzyme-linked immunosorbent assay (ELISA) technology was utilized for the quantitative analysis of specific protein expression levels. The ELISA kits were purchased from Elabscience, Houston, USA. All procedures were conducted strictly following the instructions provided by the kit manufacturer.

Immunohistochemistry and HALO quantitative analysis

Immunohistochemistry was employed to localize and quantitatively analyze specific proteins in mouse lung tissues. Following experimental treatment, mice were euthanized, and lung tissues were rapidly excised. The lung tissues were fixed in 4% paraformaldehyde solution for 24 hours, then dehydrated, cleared, and embedded in paraffin. The paraffin-embedded tissues were sectioned into continuous 4–5 μm thick slices and placed on slides. The sections underwent deparaffinization and hydration, followed by antigen retrieval using microwave treatment to expose protein epitopes. Subsequently, the sections were treated with 3% hydrogen peroxide for 10 minutes to block endogenous peroxidase activity. The sections were then blocked with 5% BSA at room temperature for 30 minutes to prevent non-specific binding. Next, the sections were incubated with primary antibodies specific to the target protein (overnight at 4°C). The following day, after washing the sections, they were incubated with the corresponding secondary antibodies for 1 hour. Color development was then performed using a diaminobenzidine (DAB) chromogen system, where DAB reacts

with hydrogen peroxide to produce a brown precipitate, marking positive signals. Finally, the nuclei were counterstained with hematoxylin and the sections were mounted.

For quantitative analysis of the immunohistochemically stained sections, HALO image analysis software was used. Images of the sections under the microscope were imported into the HALO software, and the software's built-in algorithms were employed to quantitatively analyze the positive signals of the specific protein.

ATP quantitative analysis in MPMECs

The ATP levels in MPMECs were quantitatively analyzed using an ATP Assay Kit (Elabscience, Houston, USA). Initially, MPMECs were cultured to the required density and subjected to appropriate treatments as per experimental requirements. After treatment, cells were lysed using cell lysis buffer to release ATP. To ensure efficient lysis, the lysed cells were incubated on ice for 10–15 minutes and subjected to repeated pipetting or gentle vortexing for thorough contact with the lysis buffer. Following the instructions of the ATP assay kit, the cell lysate was centrifuged (10000×g, 4 °C, for 5 minutes) to remove cell debris. The supernatant was then used for ATP measurement.

In a 96-well plate, 100 µL of sample and ATP detection reagent were added and mixed well, followed by incubation at room temperature for 5–10 minutes. The luminescence intensity was measured using a luminometer, and the ATP concentration in the samples was calculated based on a standard curve. Each sample was assayed in triplicate to ensure the accuracy and reproducibility of the results.

Immunofluorescence analysis of FAS protein in MPMECs

Immunofluorescence staining was used to analyze the expression of FAS protein in MPMECs. Initially, MPMECs were cultured on microscope-compatible slides and treated according to experimental groups. Upon reaching appropriate confluency, the cells were fixed with 4% paraformaldehyde solution for 20 minutes to preserve cellular morphology and structure. After fixation, cells were washed three times with PBS to remove the fixative. The cells were then permeabilized with 0.1% Triton X-100 for 10 minutes to allow antibody penetration.

To prevent non-specific binding, cells were blocked with 1% BSA and incubated for 30 minutes. Subsequently, the cells were incubated overnight at 4 °C with primary antibody against FAS protein (Servicebio, Wuhan, China). The next day, cells were washed with PBS to remove unbound primary antibody, followed by incubation with a fluorescently-labeled secondary antibody (Abcam, Cambridge, UK) for 1 hour. After secondary antibody incubation, cells were washed again with PBS. Finally, for nuclear staining, DAPI fluorescent dye (Beyotime, Shanghai, China) was applied. The expression and localization of FAS protein were observed and captured using a fluorescence microscope.

Mouse lung wet weight/body weight ratio

We used the mouse lung wet weight/body weight (LWW/BW) ratio to assess the extent of pulmonary edema. Initially, mice were subjected to the respective experimental treatments. After the completion of treatments, the mice were euthanized, and their body weight was accurately measured. The thoracic cavity was then immediately opened to excise the lung tissues. Upon extraction, the lung tissues were gently rinsed at room temperature with saline to remove blood and adherent materials from the lung surface, followed by gentle dabbing with filter paper to remove surface moisture. Subsequently, the lung wet weight was quickly and accurately measured using a precision electronic balance. The mouse LWW/BW ratio was calculated by dividing the lung wet weight by the body weight of the mouse, expressed in mg/g.

Evans blue permeability assay in mouse pulmonary microvasculature

To assess the permeability of the pulmonary microvasculature in mice, an Evans Blue dye assay (Solarbio, Beijing, China) was conducted. Evans Blue dye was injected to mice via the tail vein at a dosage of 30 ug/g body weight. After the dye injection, it was allowed to circulate in the system for 30 minutes. Following the injection, mice were euthanized, and lung tissues were rapidly excised. The lung tissues were first gently rinsed at room temperature with saline to remove surface blood and adherent materials. Subsequently, 100 mg of minced lung tissue was fixed in 1 mL of methanol for 24 hours to extract Evans Blue dye from the tissue. The absorbance of the solution was then measured at a wavelength of 620 nm using spectrophotometer to quantify the Evans Blue content in the lung tissues. The content of Evans Blue in the lung tissues was calculated by comparing the measured absorbance values with Evans Blue standard curve and expressed in µg/mL.

Statistical analysis

Data analysis was conducted using GraphPad Prism (Version 9.0.2). The statistical significance between the experimental and control groups was determined through the use of independent sample t-tests for pairwise comparisons and one-way ANOVA for analyses involving multiple groups. Post-hoc analysis for significant ANOVA results was carried out using Tukey test to compare means between groups. A threshold of $p < 0.05$ was established for statistical significance.

Results

Alleviation of endothelial injury in ARDS by MSCs through mitochondrial transfer

To validate the hypothesis that MSCs can alleviate endothelial injury in ARDS through mitochondrial transfer, we first examined the ability of MSCs to transfer mitochondria to MPMECs. MPMECs, which were damaged by rotenone, were co-cultured with MSCs labeled with MitoTracker Deep Red. Flow cytometry analysis confirmed the presence of MitoTracker Deep Red-labeled mitochondria in MPMECs (Figure 1(A)). Subsequently, to eliminate the possibility of false-positive results due to MitoTracker dye leakage, we damaged the mitochondria of MSCs with rotenone to inhibit their mitochondrial transfer ability. flow cytometry analysis revealed that, compared to MSCs with mitochondrial damage, normal MSCs exhibited a significantly increased mitochondria transfer rate to MPMECs (mean difference [MD]: 41.68%, 95% confidence interval [CI]: 35.4–47.94%, $p < 0.0001$) (Figure 1(B)). Following this, in vivo experiments were conducted to confirm the mitochondrial transfer from MSCs to endothelial

cells in ARDS mouse model. Immunofluorescence analysis revealed the presence of MitoTracker Deep Red-labeled mitochondria derived from MSCs within CD31-positive endothelial cells. Furthermore, HALO quantitative analysis showed that the mitochondrial transfer rate was significantly increased in the normal MSC group compared to the control group (MD: 12.52%, 95%CI: 8.56–16.48%, $P = 0.0002$) and the mitochondrial-damaged MSC group (MD: 10.50%, 95%CI: 6.54–14.46%, $P = 0.0005$) (Figure 1(C)). In addition, flow cytometry analysis of the single-cell suspension from the lung tissues of the mice also showed similar results (Figure 1(D)).

We further explored the reparative role of MSC-mediated mitochondrial transfer on endothelial damage. In vivo experiments demonstrated that intravenous injection of MSCs increased the expression of mitochondrial complex I in lung tissues of ARDS mice (Figure 1(E)). In vitro experiments also revealed that co-culturing MSCs with mitochondrially damaged MPMECs led to an increased expression of mitochondrial complex I. However, this effect was diminished when the mitochondrial transfer ability of MSCs was inhibited (Figure 1(F)). Additionally, MSCs were found to reduce ROS production (Figure 1(G)) and decrease apoptosis (Figure 1(H)) in mitochondrially damaged MPMECs. But after inhibiting mitochondrial transfer by MSCs, the effects in reducing ROS and apoptosis in MPMECs was significantly diminished. Moreover, a comparative assessment of lung tissue pathology in ARDS mice treated with normal MSCs or mitochondrial-damaged MSC revealed a reduced efficacy in repairing lung tissue pathology when mitochondrial transfer was impeded (MD of lung injury score: 2.4, 95%CI: 1.1–3.8, $P = 0.002$) (Figure 1(I)).

MSCs promote endothelial cell proliferation and vascular regeneration in ARDS lung tissue via mitochondrial transfer

To investigate whether MSCs could facilitate the proliferation of mitochondrially impaired MPMECs through mitochondrial transfer, we co-cultured MSCs with mitochondrially impaired MPMECs. Flow cytometry revealed that, compared to MSCs with mitochondrial damage, normal MSCs significantly reduced the CFSE fluorescence intensity (MD: 2004, 95%CI: 1179–2829, $P < 0.0001$) (Figure 2(A)), and increased the expression of the proliferation marker Ki67 mRNA (MD of relative expression: 2.45, 95%CI: 0.08–4.82, $P = 0.043$) in mitochondrially damaged MPMECs (Figure 2(B)). Further experiments using transwell chambers to isolate MSCs from damaged MPMECs also showed that, compared to MSCs with mitochondrial damage, normal MSCs significantly reduced CFSE fluorescence intensity (MD: 3463, 95%CI: 2753–4172, $P < 0.0001$) (Figure 2(C)) and increased the expression of Ki67 mRNA (MD of relative expression: 2.05, 95%CI: 0.83–3.27, $P = 0.003$) in damaged MPMECs (Figure 2(D)). Additionally, in vivo experiments showed that normal MSCs increased the expression of Ki67 mRNA compared to MSCs with mitochondrial damage (MD of relative expression: 1.18, 95%CI: 0.86–1.49, $P < 0.0001$) in lung tissues of ARDS mice (Figure 2(E)).

We also examined whether MSCs could promote vascular regeneration in ARDS through mitochondrial transfer. Compared to MSCs with mitochondrial damage, co-culturing mitochondrially damaged MPMECs with normal MSCs increased the expression of vascular growth factors HGF

(MD of relative expression: 2.53, 95%CI: 1.27–3.80, $P < 0.0001$) and VEGF mRNA (MD of relative expression: 2.80, 95%CI: 1.29–4.32, $P = 0.0002$) in MPMECs (Figure 2(F,G)). In addition, using transwell chambers to isolate MSCs from MPMECs, we observed a similar upregulation in the expression of HGF and VEGF mRNA in MPMECs (Figure 2(H, I)). Further in vivo experiments revealed that normal MSCs increased the expression of HGF (MD of relative expression: 2.09, 95%CI: 1.79–2.40, $P < 0.0001$) and VEGF mRNA (MD of relative expression: 2.26, 95%CI: 1.90–2.61, $P < 0.0001$) in lung tissues of ARDS mice compared to mitochondrial damaged MSCs (Figure 2(J,K)). Moreover, ELISA analysis of cell culture supernatants showed that, compared to mitochondrial damaged MSCs, normal MSCs could enhance the release of HGF (MD: 188, 95%CI: 116–259, $P < 0.0001$) and VEGF (MD: 6.7, 95%CI: 0.2–13.3, $P = 0.042$) from MPMECs (Figure 2(L,M)). Finally, immunohistochemical analysis of lung tissues revealed improved vascular integrity in ARDS mice treated with normal MSCs compared to mitochondrial damaged MSCs (Figure 2(N,O)).

MSCs transfer mitochondria to MPMECs via TNTs

To investigate whether MSCs utilize TNTs for mitochondrial transfer to MPMECs, we co-cultured mitochondria-labeled MSCs with MPMECs. Confocal microscopy observations revealed the formation of TNTs between MSCs and MPMECs (Figure 3(A)). Building upon this finding, we further examined the impact of inhibiting TNT formation on the mitochondrial transfer rate from MSCs to MPMECs. Flow cytometric analysis revealed that, compared to the control group, inhibition of TNT formation with 500nM (MD: 27.99%, 95%CI: 27.44%–28.54%, $P < 0.0001$), 1000nM (MD: 31.39%, 95%CI: 30.84%–31.94%, $P < 0.0001$), or 2000nM (MD: 31.89%, 95%CI: 32.34–33.44%, $P < 0.0001$) concentrations of Cytochalasin B significantly reduced the mitochondrial transfer rate (Figure 3(B)).

We also assessed the impact of TNT inhibition between MSCs and MPMECs on ROS production and apoptosis in mitochondrially damaged MPMECs. Flow cytometric analysis indicated that, compared to the co-culture group of MSCs and MPMECs, the addition of Cytochalasin B to the culture system to inhibit TNT formation significantly increased ROS production and apoptosis (MD of apoptosis rate: 2.3%, 95% CI: 0.7–3.9%, $P = 0.01$) in mitochondrially damaged MPMECs (Figure 3(C,D)). Furthermore, inhibition of TNT formation between MSCs and MPMECs significantly reduced the expression of mitochondrial fusion genes Mfn1 and Mfn2 mRNA in MPMECs (Figure 3(E,F)).

The adaptor protein Miro1 is a key protein involved in mitochondrial transport along TNTs. To further investigate whether MSCs transfer mitochondria to MPMECs via TNTs, we assessed the impact of TNT inhibition on Miro1 mRNA expression and then evaluated the effect of Miro1 knockdown on the mitochondrial transfer rate from MSCs to MPMECs. In vitro experiments revealed that, compared to normal MSCs, inhibition of TNT formation with Cytochalasin B significantly reduced Miro1 mRNA expression (MD of relative expression: 3.20, 95%CI: 0.83–5.57, $P = 0.014$) (Figure 3(G)). Subsequently, we constructed Miro1 knockdown MSCs, and PCR and Western blot analyses confirmed the successful knockdown of Miro1 (Figure 3(H,I)). Flow cytometry analysis revealed that, compared to normal MSCs, Miro1 knockdown MSCs exhibited a significant decrease in
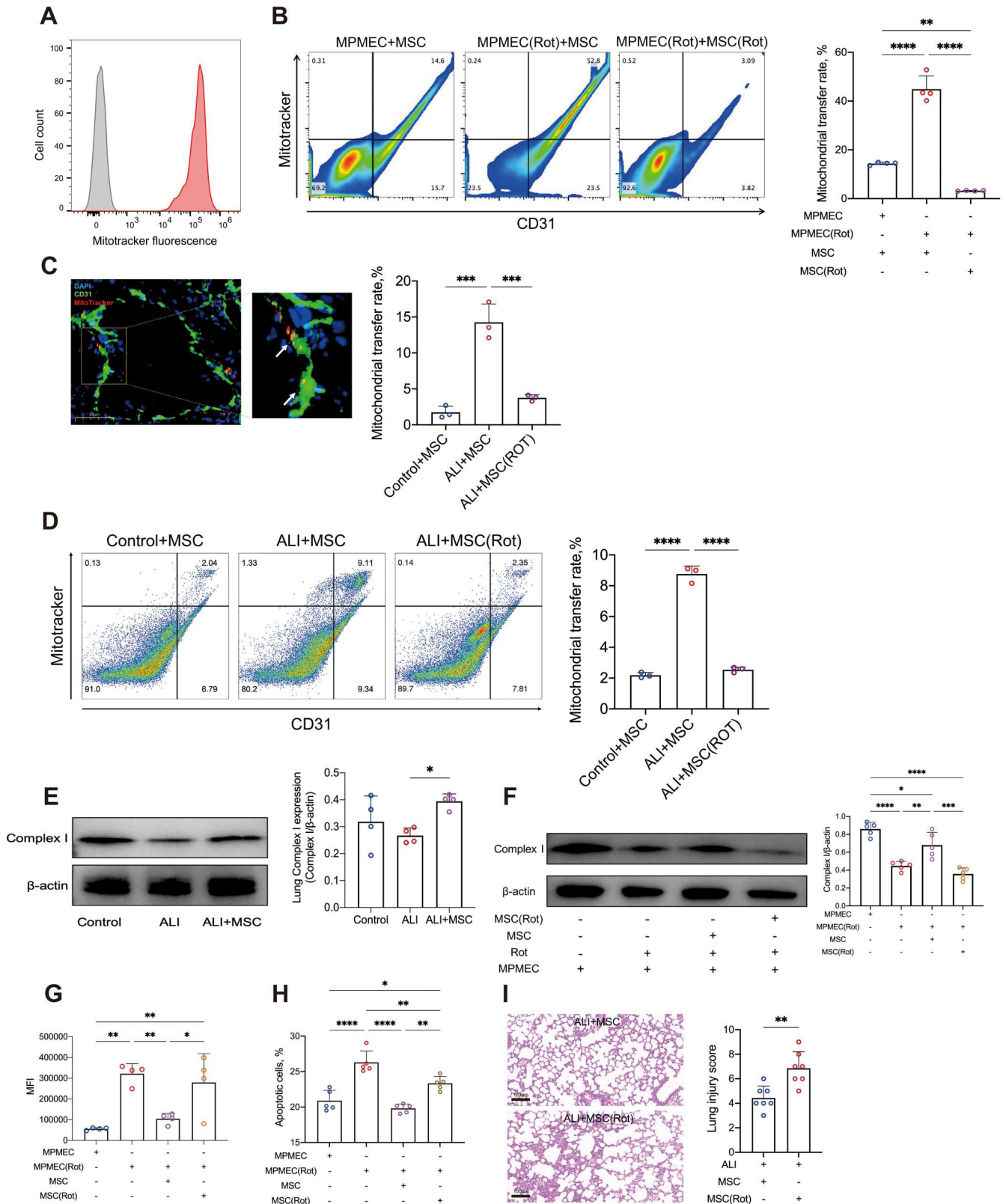
Figure 1. MSCs Mitigate Endothelial Injury in ARDS through Mitochondrial Transfer. (A) Representative flow cytometry histogram showing mitoTracker labeled mitochondrial transfer from MSCs to MPMECs ($N = 3$). Gray histogram, negative control. (B) Representative flow cytometry images and quantitative analysis of MSC-derived mitochondrial transfer to MPMECs ($N = 4$). CD31, marker for MPMECs; mitoTracker, marker for MSC-derived mitochondria. (C) Representative immunofluorescence images and HALO quantitative analysis of mouse lung tissue showing MSC-derived mitochondrial transfer to MPMECs ($N = 3$). Green signal, CD31-positive MPMECs; red signal, mitochondria derived from MSCs; blue signal, nuclei; scale bar, 50 μm. (D) Representative flow cytometry images and quantitative analysis of single-cell suspension from mouse lung tissue showing MSC-derived mitochondrial transfer to MPMECs ($N = 3$). CD31, marker for MPMECs; mitoTracker, marker for MSC-derived mitochondria. (E) Representative Western Blot images and quantitative analysis of mitochondrial complex I expression in ARDS mouse lung tissue under different conditions ($N = 4$). (F) Representative Western Blot images and quantitative analysis of mitochondrial complex I expression in MPMECs treated with different conditions ($N = 5$). (G) Flow cytometry analysis of average ROS fluorescence intensity in MPMECs treated with different conditions ($N = 4$). (H) Flow cytometry analysis of apoptosis rate in MPMECs treated with different conditions ($N = 5$). (I) Representative H&E staining images and quantitative analysis using lung injury score of lung tissues from ARDS mouse treated with MSCs or rotenone-treated MSCs ($N = 7$); scale bar, 100 μm. *$p < 0.05$, **$p < 0.01$, ***$p < 0.001$, ****$p < 0.0001$. Each dot represents an independent experiment. Error bars indicate mean ± SD.
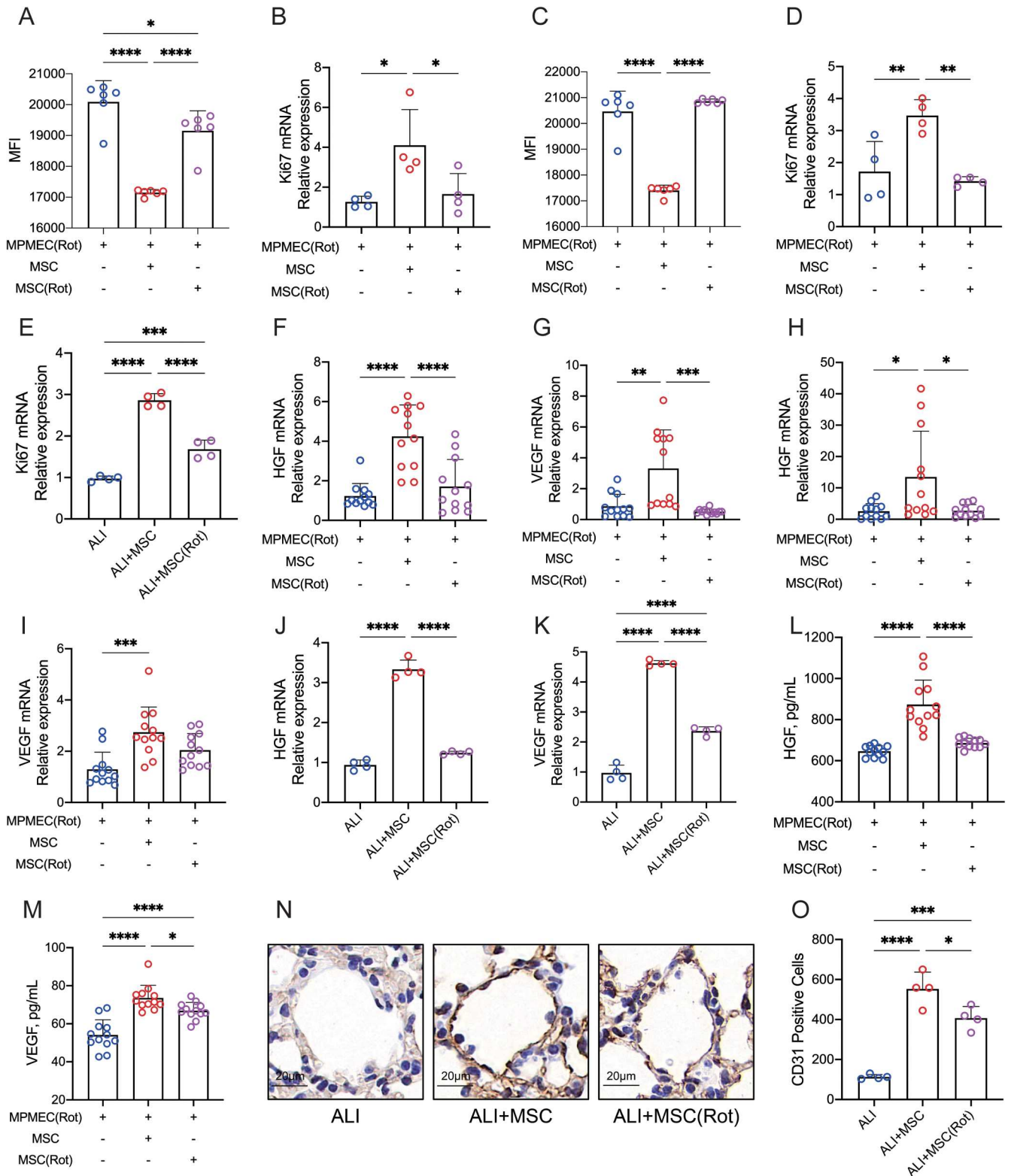
Figure 2. MSCs Promote Endothelial Cell Proliferation and Vascular Regeneration in ARDS through Mitochondrial Transfer. (A) Quantitative flow cytometry analysis of CFSE mean fluorescence intensity in mitochondrial damaged MPMECs, or co-cultured with MSCs under different conditions ($N = 5$). (B) Relative expression of cell proliferation marker Ki67 mRNA in mitochondrial damaged MPMECs, or co-cultured with MSCs under different conditions ($N = 5$). (C) Quantitative flow cytometry analysis of CFSE mean fluorescence intensity in mitochondrial damaged MPMECs, or cultured with MSCs in Transwell chambers for isolation under different conditions ($N = 5$). (D) Relative expression of Ki67 mRNA in mitochondrial damaged MPMECs, or cultured with MSCs in Transwell chambers for isolation under different conditions ($N = 4$). (E) Relative expression of Ki67 mRNA in ARDS mouse lung tissue under different conditions ($N = 4$). (F-G) Relative expression of HGF mRNA (F) and VEGF mRNA (G) in mitochondrial damaged MPMECs, or co-cultured with MSCs under different conditions ($N = 12$). (H-I) Relative expression of HGF mRNA (H) and VEGF mRNA (I) in mitochondrial damaged MPMECs, or cultured with MSCs in Transwell chambers for isolation under different conditions ($N = 12$). (J-K) Relative expression of HGF mRNA (J) and VEGF mRNA (K) in ARDS mouse lung tissue under different conditions ($N = 4$). (L-M) ELISA quantitative analysis of HGF (L) and VEGF (M) in cell culture supernatants of mitochondrial damaged MPMECs, or co-cultured with MSCs under different conditions ($N = 12$). (N-O) Representative immunohistochemical images (N) and HALO quantitative analysis (O) of lung vasculature in ARDS mice under different conditions ($N = 4$). Brown signal, endothelial cells; blue signal, nuclei; scale bar, 20 μm. $*p < 0.05$, $**p < 0.01$, $***p < 0.001$, $****p < 0.0001$. Each dot represents an independent experiment. Error bars indicate mean ± SD.
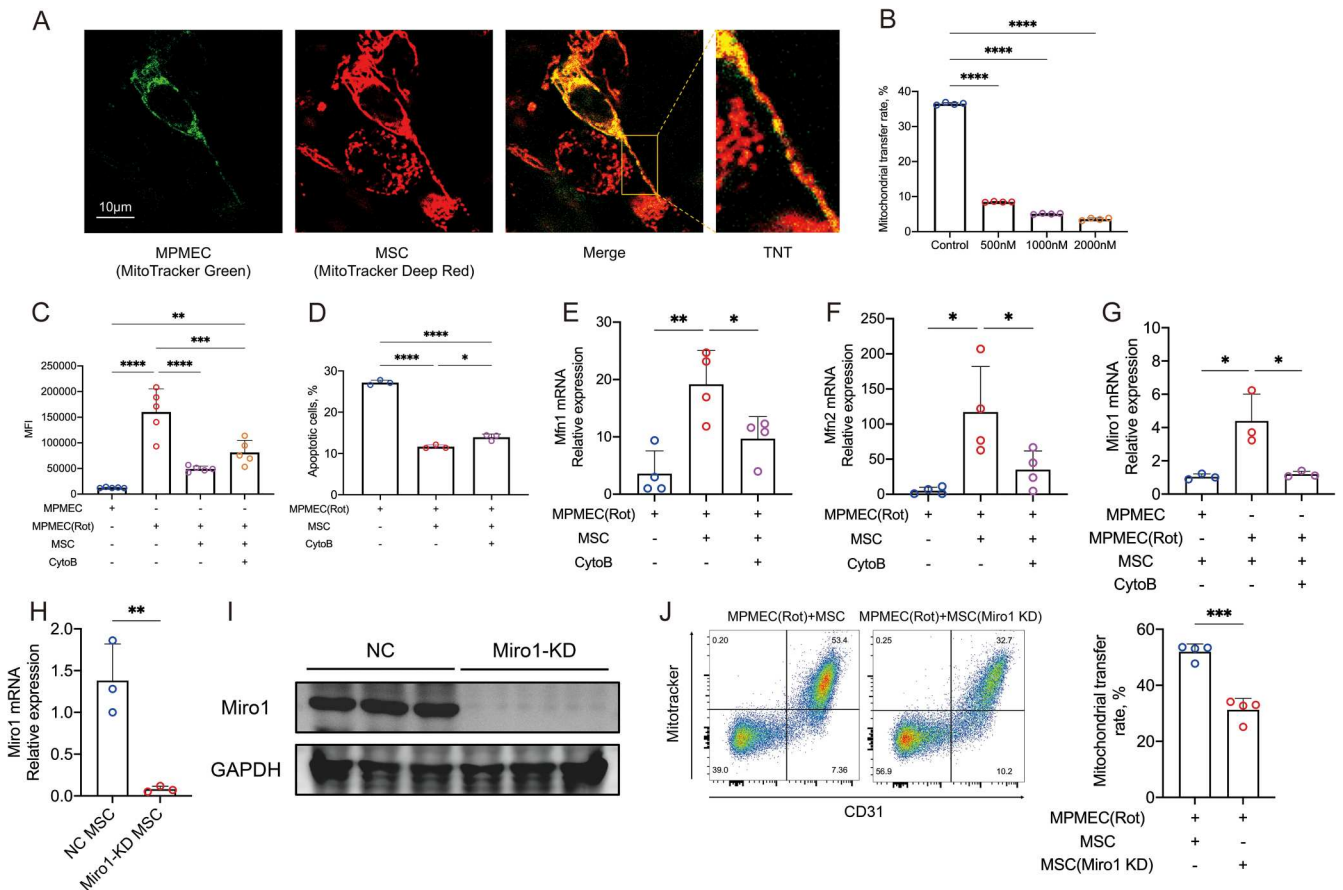
Figure 3. MSCs Transfer Mitochondria to MPMECs via TNTs. (A) Representative confocal microscopy image showing mitochondrial transfer from MSCs to MPMECs via TNTs ($N = 3$). Red signal, MSCs; green signal, MPMECs; enlarged section, TNT; scale bar, 10 μm. (B) Flow cytometry quantification of mitochondrial transfer rate from MSCs to MPMECs in co-culture systems with different concentrations of Cytochalasin B ($N = 4$). (C) Quantitative flow cytometry analysis of ROS in MPMECs treated with different conditions ($N = 5$). (D) Quantitative flow cytometry analysis of apoptosis in mitochondrial damaged MPMECs, or co-cultured with MSCs under different conditions ($N = 3$). (E-F) Relative expression of Mfn1 mRNA (E) and Mfn2 mRNA (F) in mitochondrial damaged MPMECs, or co-cultured with MSCs under different conditions ($N = 4$). (G) Relative expression of Miro1 mRNA in MSCs co-cultured with MPMECs under different conditions ($N = 3$). (H-I) Relative expression of Miro1 mRNA (H) and Miro1 protein (I) in negative control MSCs and Miro1 knockdown MSCs ($N = 3$). (J) Representative flow cytometry images and quantitative analysis of mitochondrial transfer rate from negative control MSCs or Miro1 knockdown MSCs to mitochondrial damaged MPMECs ($N = 4$). CD31, marker for MPMECs; mitoTracker, marker for MSC-derived mitochondria. $*p < 0.05$, $**p < 0.01$, $***p < 0.001$, $****p < 0.0001$. Each dot represents an independent experiment. Error bars indicate mean ± SD.

mitochondrial transfer rate to mitochondrial damaged MPMECs (MD: 20.73%, 95% CI: 14.68–26.77%, $P = 0.0002$) (Figure 3(J)).

MPMECs uptake mitochondria from MSCs via dynamin-dependent clathrin-mediated endocytosis

To investigate whether MSCs transfer mitochondria to MPMECs under isolated conditions, we cultured mitochondria-prelabeled MSCs and MPMECs separately using transwell chamber. Fluorescence microscopy revealed that mitochondria from MSCs were localized in MPMECs (Figure 4(A)). Further experiments discovered that under isolated culture conditions, the mitochondrial transfer from MSCs to MPMECs could be inhibited by dynasore, a dynamin-dependent clathrin-mediated endocytosis inhibitor (Figure 4(B)). We further assessed the impact of inhibiting endocytosis on ROS production and apoptosis in mitochondrially damaged MPMECs, and found that, compared to control group, inhibition of endocytosis in MPMECs significantly weakened the ability of MSCs to reduce ROS production and apoptosis (MD of apoptosis rate: 5.8%, 95%CI: 2.5–9.1%, $P = 0.001$) in mitochondrially damaged MPMECs (Figure 4(C,D)). Additionally, compared to the group where mitochondrially damaged MPMECs were cultured separately

from MSCs, inhibition of endocytosis in MPMECs significantly reduced the expression of Mfn1 (MD of relative expression: 10.46, 95%CI: 0.17–20.74, $P = 0.046$) and Mfn2 mRNA (MD of relative expression: 5.89, 95%CI: 2.33–9.44, $P = 0.003$) (Figure 4(E,F)).

Mitochondrial transfer from MSCs to MPMECs enhances fatty acid synthesis, facilitating vascular regeneration in ARDS

To elucidate the mechanism by which MSCs promote vascular regeneration in ARDS through mitochondrial transfer, we first examined whether MSCs alter the energy metabolism of MPMECs via mitochondrial transfer. In vitro experiments revealed that MSCs were able to increase ATP production in MPMECs. However, inhibition of mitochondrial transfer from MSCs did not significantly decrease ATP production in MPMECs (Figure 5(A)). Fatty acid synthesis plays an important role in vascular regeneration. Therefore, we further investigated whether MSCs regulate fatty acid synthesis in MPMECs through mitochondrial transfer, thereby promoting vascular regeneration. In vitro experiments showed that, compared to MSCs with inhibited mitochondrial transfer ability, normal MSCs significantly increased the expression of key enzymes involved
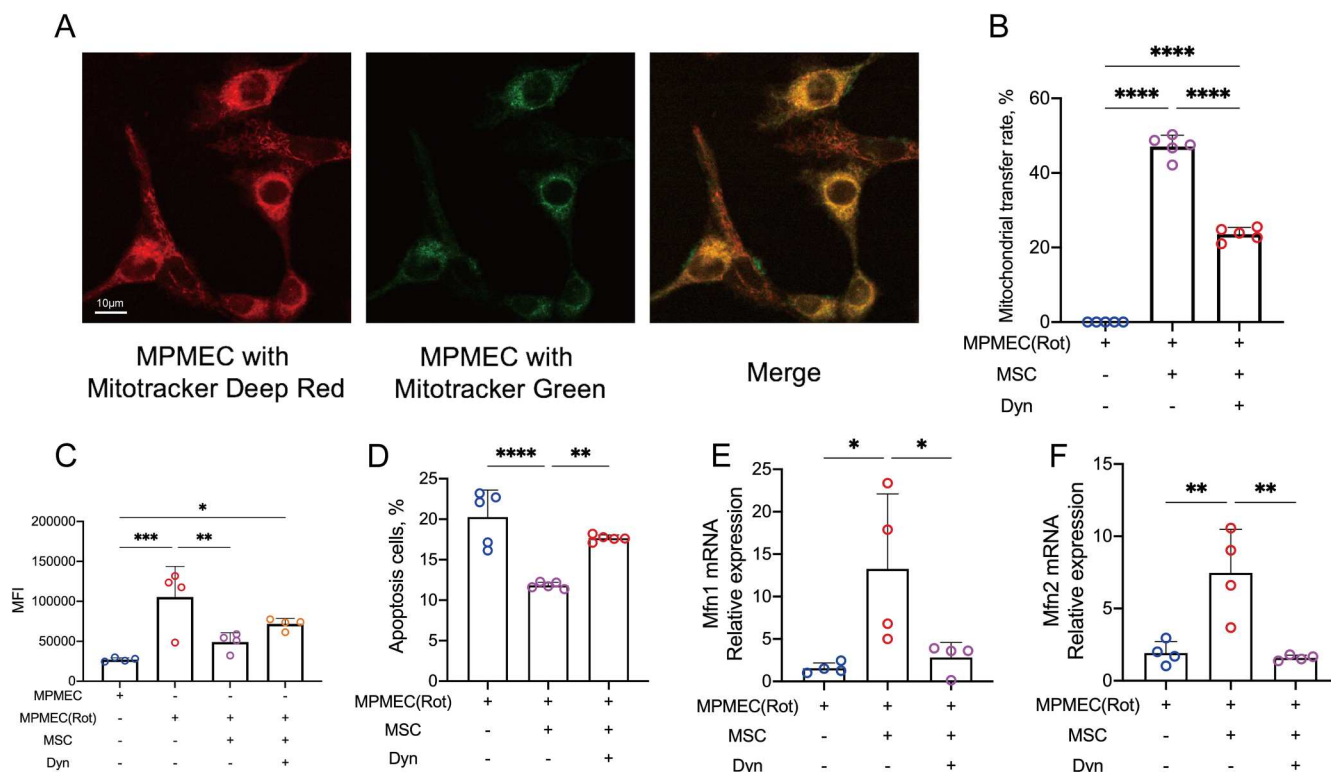
Figure 4. MPMECs Accept Mitochondria from MSCs through Dynamin-Dependent Clathrin-Mediated Endocytosis. (A) Representative fluorescence microscopy image showing mitochondrial transfer from MSCs to mitochondrial damaged MPMECs cultured in Transwell chambers for isolation ($N = 3$). Red signal, mitochondria of MPMECs; green signal, mitochondria from MSCs; scale bar, 10 μm. (B) Flow cytometry quantification of mitochondrial transfer rate from MSCs to mitochondrial damaged MPMECs cultured in Transwell chambers for isolation under different conditions ($N = 5$). (C) Quantitative flow cytometry analysis of ROS in MPMECs, or cultured with MSCs in Transwell chambers for isolation under different conditions ($N = 4$). (D) Quantitative flow cytometry analysis of apoptosis in mitochondrial damaged MPMECs, or cultured with MSCs in Transwell chambers for isolation under different conditions ($N = 5$). (E-F) Relative expression of Mfn1 mRNA (E) and Mfn2 mRNA (F) in mitochondrial damaged MPMECs, or cultured with MSCs in Transwell chambers for isolation under different conditions ($N = 4$). *$p < 0.05$, **$p < 0.01$, ***$p < 0.001$, ****$p < 0.0001$. Each dot represents an independent experiment. Error bars indicate mean ± SD.

in fatty acid synthesis, including FAS (MD of relative expression: 6.67, 95%CI: 4.12–9.23, $P = 0.0001$), ACC (MD of relative expression: 4.47, 95%CI: 2.40–6.53, $P = 0.0005$), and ACLY (MD of relative expression: 8.01, 95%CI: 4.80–11.21, $P = 0.0002$) mRNA, in mitochondrially damaged MPMECs (Figure 5(B–D)). Further in vivo experiments confirmed that, compared to MSCs with inhibited mitochondrial transfer ability, normal MSCs increased the expression of these key enzymes in fatty acid synthesis in lung tissues of ARDS mice (Figure 5(E–G)).

To further validate that MSCs mediate vascular regeneration by regulating fatty acid synthesis in MPMECs, We first validated the inhibitory effect of C75, a fatty acid synthase inhibitor, on fatty acid synthesis in MPMECs. Immunofluorescence staining confirmed that C75 effectively inhibited FAS expression and cell proliferation (Figure 5(H)). Subsequently, we examined the effect of inhibiting fatty acid synthesis on the expression of angiogenic factors VEGF and HGF mRNA in MPMECs. We found that, compared to mitochondrially damaged MPMECs co-cultured with MSCs, the addition of C75 significantly decreased the expression of VEGF (MD of relative expression: 1.72, 95%CI: 1.34–2.10, $P < 0.0001$) and HGF (MD of relative expression: 4.58, 95%CI: 0.41–8.74, $P = 0.03$) mRNA in MPMECs (Figure 5(I,J)). Furthermore, the addition of C75 also significantly reduced the concentration of VEGF and HGF proteins in the cell culture supernatant (Figure 5(K,L)). Overall, these findings substantiate the role of MSCs in mediating vascular regeneration in ARDS through the regulation of fatty acid synthesis via mitochondrial transfer.

Stimulation of the TCA cycle by MSC-Transferred mitochondria activates citrate-dependent fatty acid synthesis in MPMECs

The mechanism by which MSCs regulate fatty acid synthesis in MPMECs after transferring mitochondria remains unclear. Given that mitochondria are central to the TCA cycle, an upstream pathway of fatty acid synthesis, we first investigated whether MSC-mediated mitochondrial transfer stimulates the TCA cycle in MPMECs. In vitro experiments revealed that, compared to MPMECs co-cultured with normal MSCs, the expression of key TCA cycle enzymes, including CS (MD: 23.76, 95%CI: 2.82–44.70, $P = 0.032$), IDH (MD: 3.20, 95%CI: 1.82–4.56, $P = 0.001$), and OGDH (MD: 11.16, 95%CI: 1.26–21.07, $P = 0.03$) mRNA, was significantly reduced in MPMECs co-cultured with MSCs treated with rotenone (Figure 6(A–C)). Subsequently, we used Devimistat to inhibit the TCA cycle and observed the impact of TCA cycle inhibition on fatty acid synthesis in MPMECs. In vitro experiments confirmed that Devimistat effectively reduced CS mRNA expression in MPMECs (Figure 6(D)). Further experiments revealed that inhibiting the TCA cycle in MPMECs significantly reduced the expression of key fatty acid synthesis enzymes, including FAS, ACC, and ACLY mRNA, in MPMECs co-cultured with MSCs (Figure 6(E–G)).

Citrate, a critical link between cellular TCA cycle and fatty acid synthesis, was also tested. Immunofluorescence analysis of FAS indicated that inhibiting the TCA cycle reduced FAS expression and cell proliferation, whereas the addition of citrate increased FAS expression in MPMECs (Figure 6(H)).
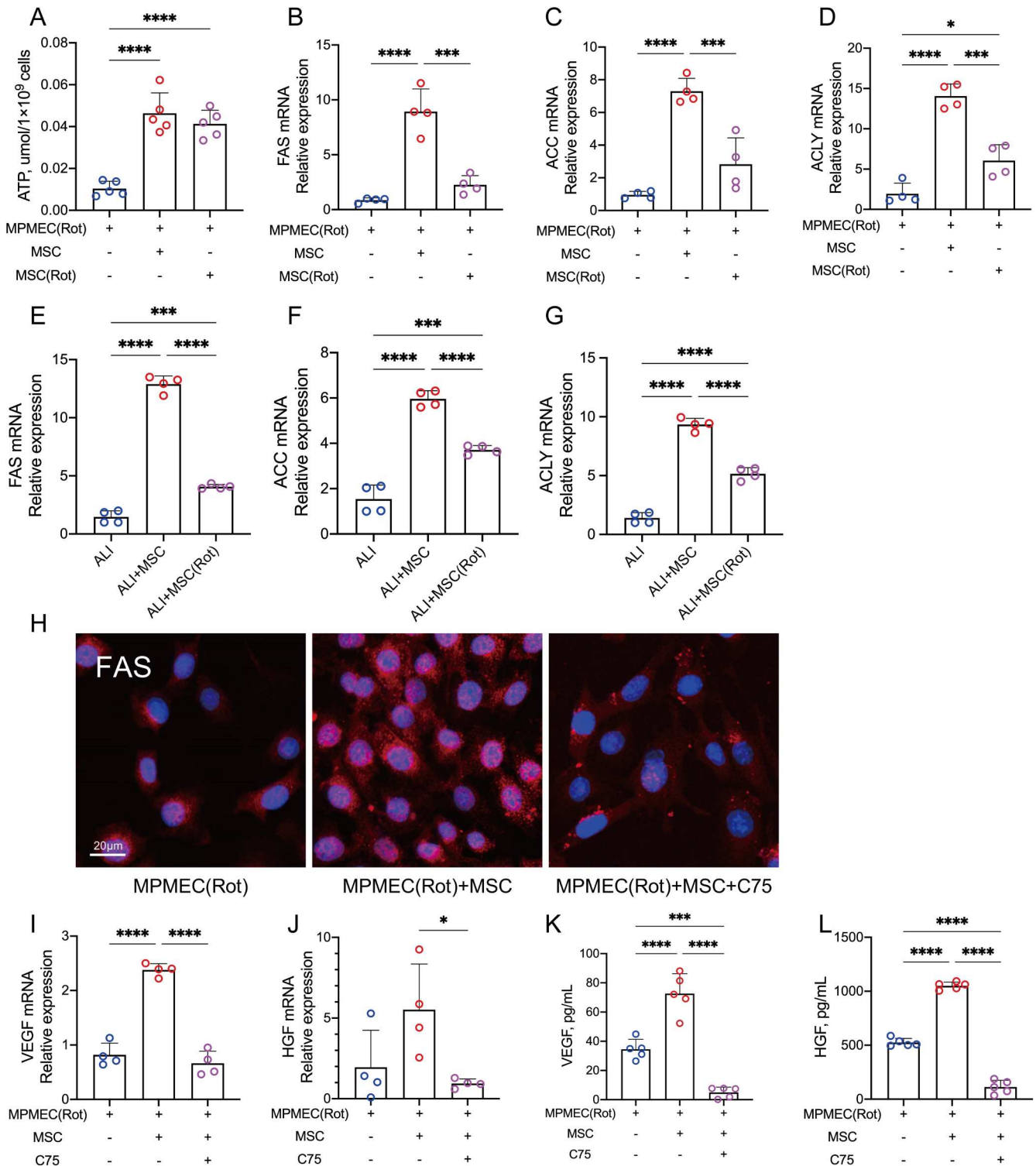
Figure 5. MSCs Transfer Mitochondria to MPMECs Promoting Fatty Acid Synthesis and Vascular Regeneration. (A) Quantitative analysis of ATP in mitochondrial damaged MPMECs, or co-cultured with MSCs under different conditions ($N = 5$). (B-D) Relative expression of key fatty acid synthesis enzyme FAS mRNA (B), ACC mRNA (C), ACLY mRNA (D) in mitochondrial damaged MPMECs, or co-cultured with MSCs under different conditions ($N = 4$). (E-G) Relative expression of key fatty acid synthesis enzyme FAS mRNA (E), ACC mRNA (F), ACLY mRNA (G) in lung tissues of ARDS mice, or treated with MSCs under different conditions ($N = 4$). (H) Representative immunofluorescence images of FAS in mitochondrial damaged MPMECs, or co-cultured with MSCs under different conditions ($N = 3$). Red signal, FAS; blue signal, nuclei; scale bar, 20 μm. (I-J) Relative expression of VEGF mRNA (I) and HGF mRNA (J) in mitochondrial damaged MPMECs, or co-cultured with MSCs under different conditions ($N = 4$). (K-L) ELISA quantitative analysis of VEGF (K) and HGF (L) in cell culture supernatants of mitochondrial damaged MPMECs, or co-cultured with MSCs under different conditions ($N = 5$). *$p < 0.05$, **$p < 0.01$, ***$p < 0.001$, ****$p < 0.0001$. Each dot represents an independent experiment. Error bars indicate mean ± SD.

Further PCR analysis of FAS, ACC, and ACLY mRNA expression revealed that citrate partially restored the expression of these key enzymes involved in fatty acid synthesis after TCA cycle inhibition in MPMECs (Figure 6(I–K)). These findings collectively confirm that mitochondrial transfer from MSCs to MPMECs stimulates the TCA cycle, thereby activating citrate-dependent fatty acid synthesis.

Citrate restores the angiogenic potential of mitochondrially damaged MSCs

To explore the role of citrate in restoring the angiogenic potential of mitochondrially impaired MSCs in ARDS, we first conducted in vitro experiments to observe the effects of citrate on fatty acid synthesis in MPMECs co-cultured

with damaged MSCs. PCR quantification analysis revealed that, compared to mitochondrially impaired MSCs alone, the addition of citrate significantly increased the expression of key fatty acid synthesis enzymes FAS, ACC (MD: 1.48, 95%CI: 0.33–2.63, $P = 0.014$), and ACLY (MD: 3.18, 95%CI: 1.74–4.61, $P = 0.0004$) mRNA in MPMECs (Figure 7(A–C)). Further, we examined whether citrate could restore the angiogenic function of damaged MSCs. PCR analysis of MPMECs revealed that, compared to mitochondrially impaired MSCs alone, the addition of citrate significantly increased the expression of angiogenic factors VEGF (MD: 1.58, 95%CI: 0.70–2.45, $P = 0.002$) and HGF (MD: 0.81, 95%CI: 0.41–1.21, $P = 0.0008$) mRNA in mitochondrially impaired MPMECs (Figure 7(D,E)). Additionally, ELISA-based quantification of VEGF and HGF proteins in the cell culture supernatant also revealed that citrate can partially restore the ability of damaged MSCs to promote MPMEC-mediated angiogenic factor release (Figure 7(F,G)).

Further in vivo experiments were conducted to observe the effect of citrate in restoring the angiogenic potential of damaged MSCs and in repairing lung injury in ARDS. The results showed that intravenous injection of MSCs reduced lung injury and improved the integrity of lung tissue vasculature in ARDS mice. This reparative effect was diminished when the mitochondrial transfer ability of MSCs was inhibited. However, treating damaged MSCs with citrate enhanced their protective effect on lung injury and vascular integrity in ARDS mice (Figure 7(H)). These findings collectively confirm that citrate can restore the angiogenic potential of mitochondrially impaired MSCs.

MSCs alleviate LPS-Induced lung injury

Finally, we evaluated the reparative effects of MSCs on LPS-induced lung injury. H&E staining of lung tissue and quantitative analysis of lung injury score revealed that, compared to untreated ARDS mice, intravenous administration of MSCs significantly reduced pulmonary pathological damage in ARDS mice (Figure 8(A,B)). Additionally, immunohistochemical staining and quantitative analysis using HALO software for the endothelial cell adhesion protein Occludin showed that MSC treatment significantly increased Occludin expression in the lung tissue of ARDS mice compared to untreated ARDS mice (Figure 8(C,D)). Further, we observed that, compared to untreated ARDS mice, MSC treatment significantly decreased inducible nitric oxide synthase (iNOS) expression (MD: 94.58, 95%CI: 4.50–184.70, $P = 0.037$) and increased endothelial nitric oxide synthase (eNOS) expression (MD: 8.96, 95%CI: 3.61–14.31, $P = 0.008$) in the lung tissue of ARDS mice (Figure 8(E,F)). Building on this, we further examined the effects of MSC treatment on pulmonary edema in ARDS mice (assessed by LWW/BW ratio) and pulmonary capillary permeability (evaluated using Evans blue permeability assay). The results showed that, compared to untreated ARDS mice, MSC treatment significantly reduced the LWW/BW ratio (MD: 2.6, 95% CI: 0.6–4.6, $P = 0.01$) and the concentration of Evans blue (MD: 1.89, 95%CI: 1.35–2.43, $P < 0.0001$) in ARDS lung tissue (Figure 8(G,H)). In summary, our findings demonstrate that MSCs can effectively alleviate lung injury in ARDS.

Discussion

ARDS is a severe pulmonary inflammatory response characterized primarily by extensive alveolar damage and capillary leakage. Mitochondrial dysfunction in lung tissue cells plays a critical role in the pathophysiology of ARDS due to inflammation and oxidative stress [26]. Currently, there is a lack of effective treatments specifically targeting mitochondrial damage in ARDS. MSCs, a type of pluripotent stem cells, have gained attention for their potential in tissue repair, immunomodulation, and anti-inflammatory actions [27]. Our study demonstrates that MSCs can repair mitochondrial damage in ARDS endothelial cells through mitochondrial transfer. This process activates the TCA cycle and fatty acid synthesis, leading to enhanced cell proliferation and the release of pro-angiogenic factors in endothelial cells, which subsequently promote vascular regeneration. These findings provide a novel perspective on ARDS treatment, underscoring the therapeutic potential of MSCs in mitigating mitochondrial damage in ARDS pulmonary endothelial cells and enhancing vascular repair.

Mitochondrial transfer is a critical mechanism by which MSCs repair mitochondrial injury in ARDS pulmonary endothelial cells. Since Spees et al. first described mitochondrial transfer in 2006 [16], this phenomenon has gained increasing attention for its role in regulating cellular metabolism, tumor growth, mitochondrial quality control, wound healing, and immune modulation [18]. MSCs represent a promising cellular therapy for ARDS, and recent studies have shown that MSCs can transfer mitochondria to ARDS alveolar epithelial cells [20], T lymphocytes [23,28], and macrophages [22], thereby facilitating tissue repair [29,30]. Our study further reveals that MSCs can transfer mitochondria to ARDS pulmonary endothelial cells, a key process in mitigating endothelial mitochondrial damage and providing a novel therapeutic approach for repairing mitochondrial injury in ARDS endothelial cells.

TNTs serve as an important mechanism for MSCs to transfer mitochondria to ARDS pulmonary endothelial cells. TNTs represent a specialized form of intercellular communication, consisting of long, thin cellular protrusions that allow direct transfer of organelles and signaling molecules between cells [31]. In our research, TNTs formed a 'bridge' between MSCs and MPMECs, enabling MSCs to directly transfer mitochondria to mitochondrially impaired MPMECs. Previous studies support the critical role of TNTs in mitochondrial transfer [32,33]. One study demonstrated that cardiomyocytes transfer mitochondria to adjacent damaged cells via TNTs [34]. Similarly, research has shown that microglial cells use TNTs to transfer mitochondria to neuronal cells, thereby enhancing cell survival and stabilizing neural networks [35,36].

The disruption of the pulmonary capillary barrier is a key pathological feature of ARDS, leading to non-cardiogenic pulmonary edema [37]. Following damage to the pulmonary endothelial cells in ARDS, the release of angiogenic factors is reduced, impairing the endothelial repair capacity [38]. MSC-mediated mitochondrial transfer enhances the release of angiogenic factors from ARDS pulmonary endothelial cells, promoting vascular repair and maintaining pulmonary capillary barrier function, which plays a critical role in lung injury recovery in ARDS [39,40].

Fatty acid synthesis is a key metabolic pathway in MSC-mediated mitochondrial transfer that promotes pulmonary vascular regeneration in ARDS. As a crucial aspect of cellular metabolism, fatty acid synthesis plays an essential role not only in energy storage and provision but also in various
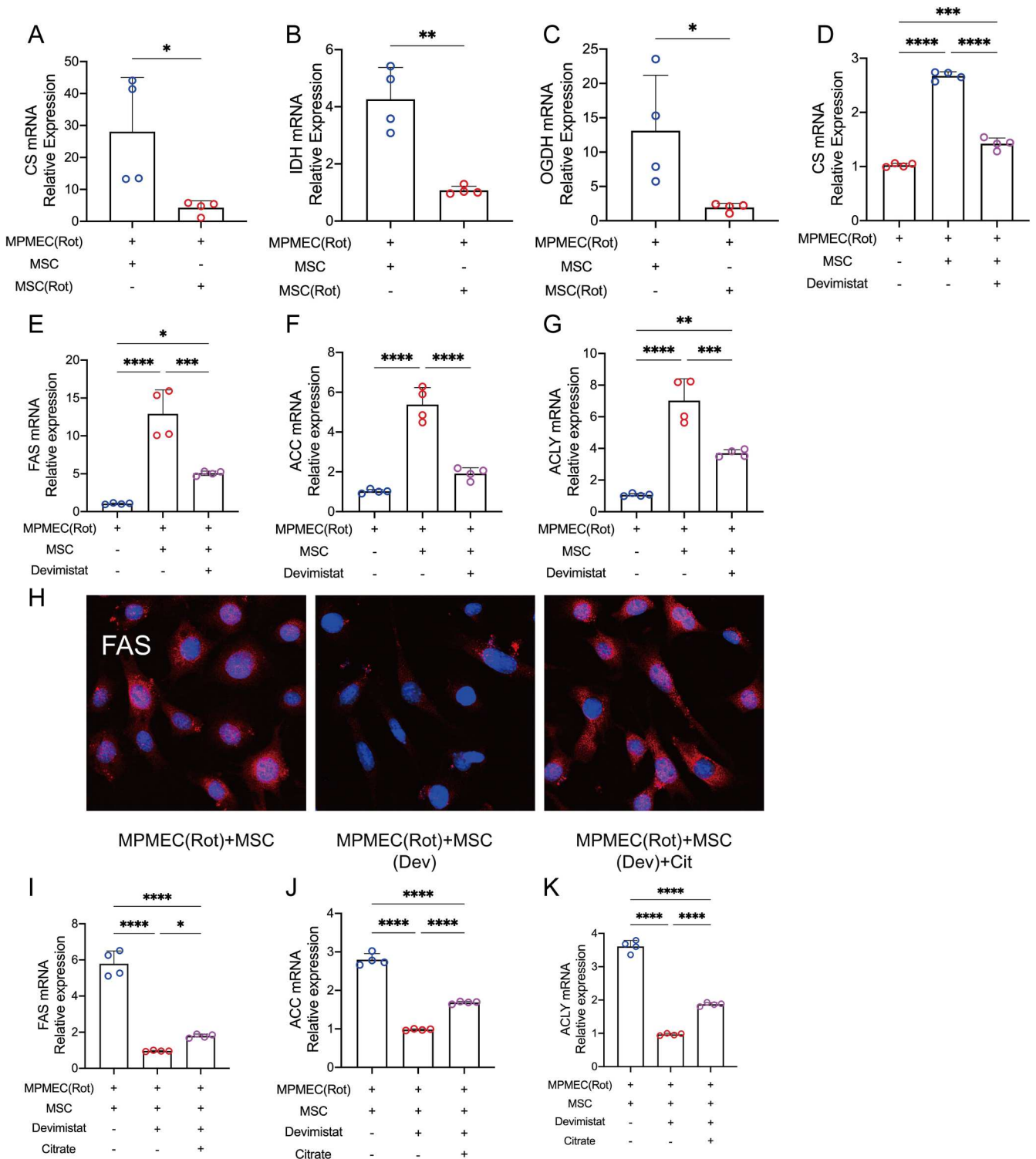
Figure 6. MSCs Transfer Mitochondria to MPMECs Stimulating the TCA Cycle and Activating Citrate-Dependent Fatty Acid Synthesis. (A-C) Relative expression of the key TCA cycle enzyme CS mRNA (A), IDH mRNA (B) and OGDH mRNA (C) in mitochondrial damaged MPMECs, or co-cultured with MSCs under different conditions ($N = 4$). (D) Relative expression of CS mRNA in mitochondrial damaged MPMECs, or co-cultured with MSCs with or without Devimistat ($N = 4$). (E-G) Relative expression of key fatty acid synthesis enzyme FAS mRNA (E), ACC mRNA (F) and ACLY mRNA (G) in mitochondrial damaged MPMECs, or co-cultured with MSCs with or without Devimistat ($N = 4$). (H) Representative immunofluorescence images of FAS in mitochondrial damaged MPMECs co-cultured with MSCs under different conditions ($N = 3$). Red signal, FAS; blue signal, nuclei. (I-K) Relative expression of key fatty acid synthesis enzyme FAS mRNA (I), ACC mRNA (J) and ACLY mRNA (K) in mitochondrial damaged MPMECs co-cultured with MSCs under different conditions ($N = 4$). $*p < 0.05$, $**p < 0.01$, $***p < 0.001$, $****p < 0.0001$. Each dot represents an independent experiment. Error bars indicate mean $\pm$ SD.

cellular functions [41]. Studies have shown that fatty acid synthesis provides vital biomolecular components for endothelial cells and directly influences their proliferation [42]. Additionally, fatty acid synthesis affects endothelial cell function and survival, maintains vascular integrity, and promotes repair after injury [43]. Moreover, fatty acids act as signaling molecules, regulating intracellular pathways and influencing

cellular behavior, including the release of angiogenic factors [44,45].

The TCA cycle serves as a crucial link in MSC-mediated mitochondrial transfer that promotes fatty acid synthesis in ARDS endothelial cells. Previous studies have highlighted the importance of TCA cycle activity in maintaining anabolic metabolism, particularly in rapidly proliferating cells [46]. As a
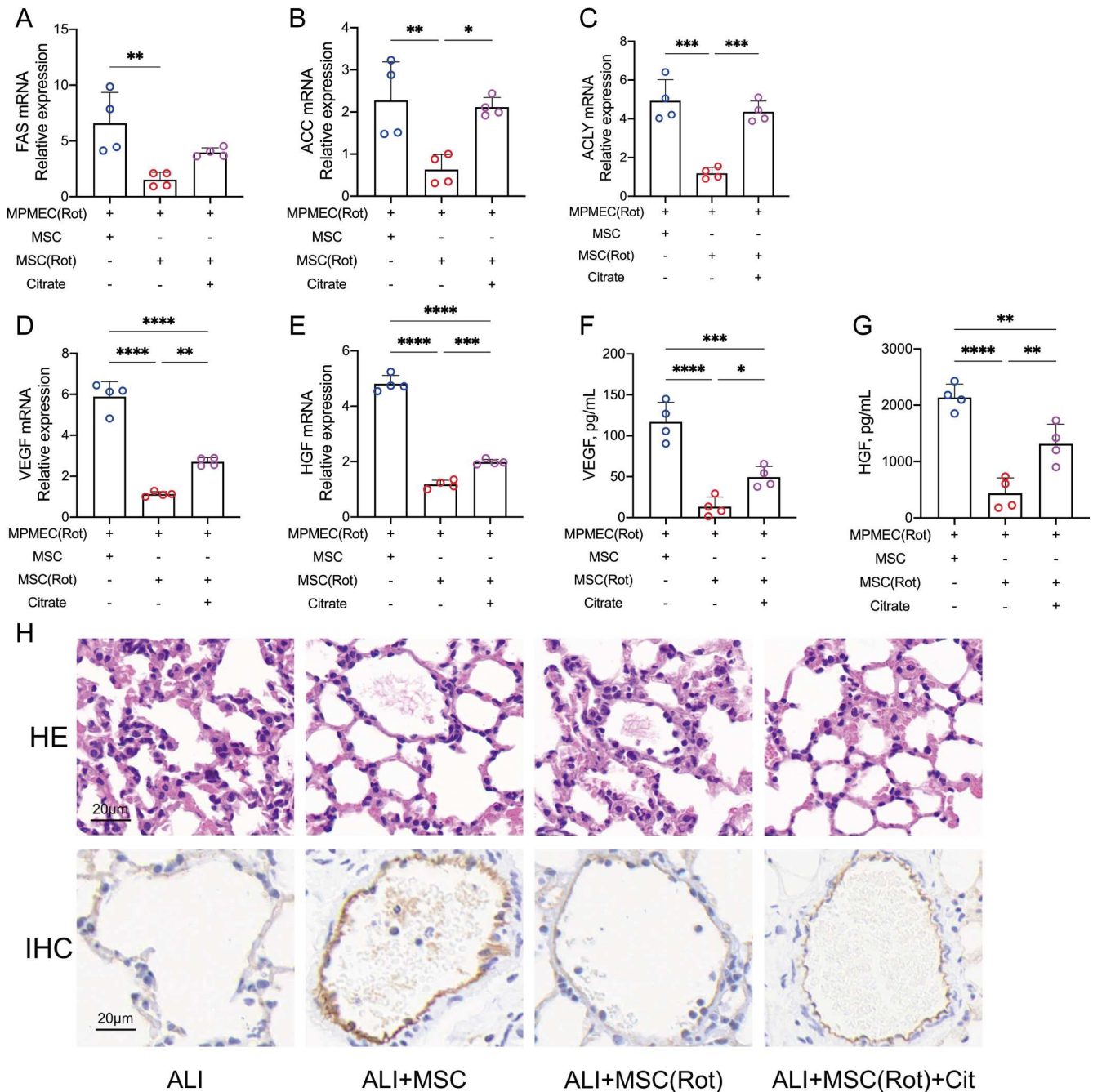
Figure 7. Citrate Restores the Vascular Regenerative Function of Mitochondrially Damaged MSCs. (A-C) Relative expression of key fatty acid synthesis enzyme FAS mRNA (A), ACC mRNA (B) and ACLY mRNA (C) in mitochondrial damaged MPMECs co-cultured with MSCs under different conditions ($N = 4$). (D-E) Relative expression of VEGF mRNA (D) and HGF mRNA (E) in mitochondrial damaged MPMECs co-cultured with MSCs under different conditions ($N = 4$). (F-G) ELISA quantitative analysis of VEGF (F) and HGF (G) in cell culture supernatants of mitochondrial damaged MPMECs co-cultured with MSCs under different conditions ($N = 4$). (H) Representative images of H&E staining (top row) and endothelial cell immunohistochemical analysis (bottom row) of lung tissue in ARDS mice, or treated with MSCs under different conditions ($N = 3$). The brown signal indicates endothelial cells; the blue signal indicates nuclei; scale bar, 20 μm. *$p < 0.05$, **$p < 0.01$, ***$p < 0.001$, ****$p < 0.0001$. Each dot represents an independent experiment. Error bars indicate mean ± SD.

key biosynthetic process, fatty acid synthesis relies on the raw materials and energy provided by the TCA cycle. Moreover, citrate, an essential component of the TCA cycle, is not only a critical intermediate in energy metabolism but also a vital precursor for fatty acid synthesis [47]. Citrate can exit the mitochondria and enter the cytoplasm, where it is converted by citrate lyase into acetyl-CoA, a direct substrate for fatty acid synthesis.

This study has several limitations. Firstly, we utilized Mito-Tracker to label MSC mitochondria for the observation of mitochondrial transfer. However, a known limitation of Mito-Tracker is the potential for dye leakage, which may lead to false-positive results. To minimize this risk, we incorporated multiple control groups to rigorously exclude the possibility of false-positive signals caused by dye leakage. Nevertheless, we acknowledge that despite these precautions, the potential influence of dye diffusion cannot be entirely ruled out, and future studies employing genetically encoded mitochondrial reporters may further validate our findings. Secondly, this study primarily relies on ARDS mouse model and cell model, which may limit the direct applicability of the findings to humans. Thirdly, the observation of MPMECs accepting mitochondria from MSCs through dynamin-dependent clathrin-mediated endocytosis mainly relies on the use of the endocytosis inhibitor Dynasore. While the inhibition of endocytosis with Dynasore allows for indirect inference
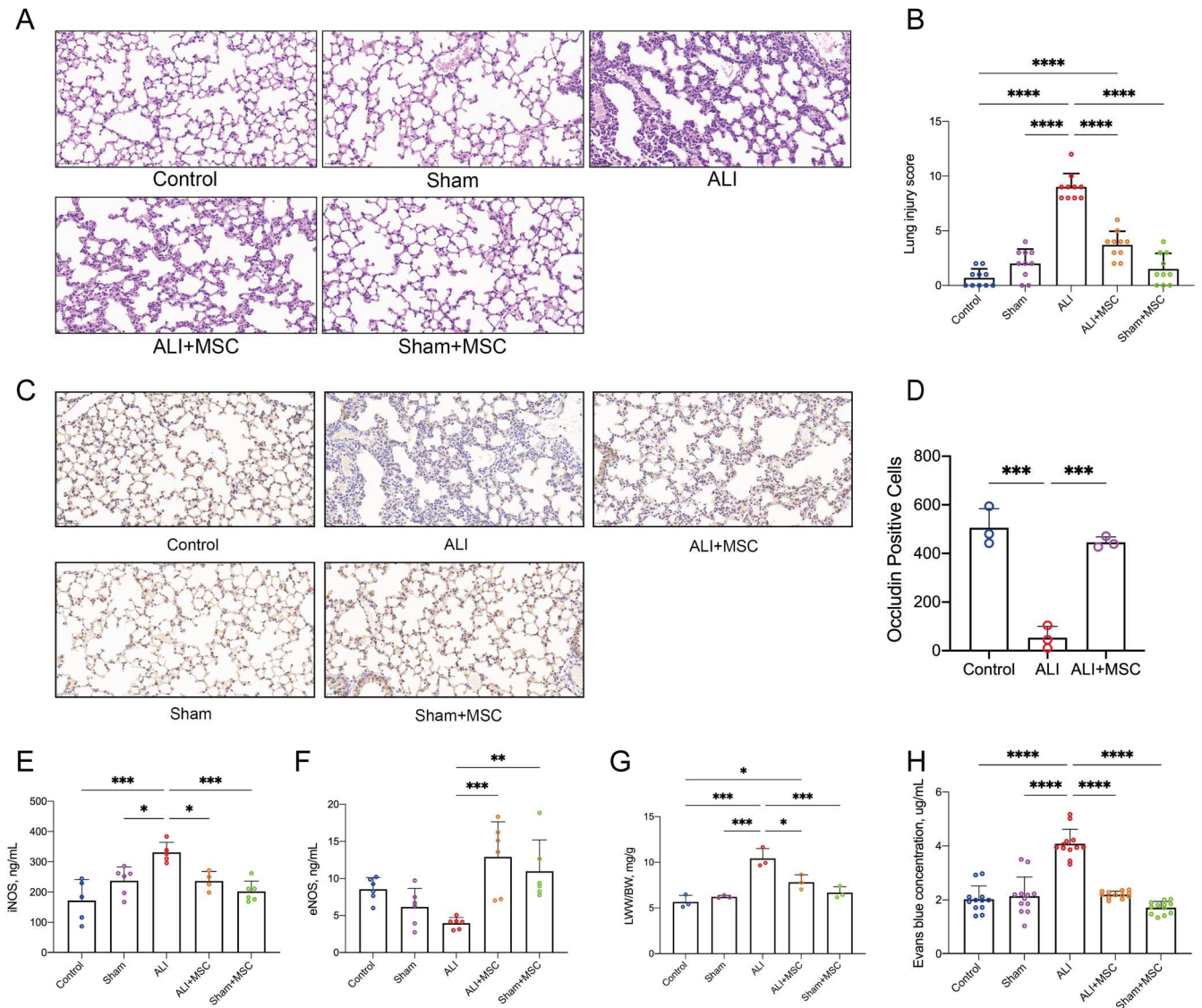
Figure 8. MSCs Alleviate LPS-Induced Lung Injury. (A–B) Representative H&E-stained images (A) and quantitative analysis of lung injury score (B) of lung tissues from normal mice, sham-operated, ARDS, ARDS treated with MSCs, and sham-operated mice treated with MSCs ($N = 3$). Scale bar, 50 μm. (C) Representative immunohistochemical images of endothelial cell adhesion protein Occludin in lung tissues from normal mice, sham-operated, ARDS, ARDS treated with MSCs, and sham-operated mice treated with MSCs ($N = 3$). Brown signal, Occludin-positive signal; blue signal, nuclei; scale bar, 50 μm. (D) HALO quantitative analysis of Occludin immunohistochemistry in lung tissues from normal mice, ARDS, and ARDS treated with MSCs ($N = 3$). (E-F) ELISA quantitative analysis of iNOS (E) and eNOS (F) expression in lung tissues from normal mice, sham-operated, ARDS, ARDS treated with MSCs, and sham-operated mice treated with MSCs. (G) The LWW/BW ratio from normal mice, sham-operated, ARDS, ARDS treated with MSCs, and sham-operated mice treated with MSCs ($N = 3$). (H) Evans blue content in lung tissues from normal mice, sham-operated, ARDS, ARDS treated with MSCs, and sham-operated mice treated with MSCs. *$p < 0.05$, **$p < 0.01$, ***$p < 0.001$, ****$p < 0.0001$. Each dot represents an independent experiment. Error bars indicate mean ± SD.

of mitochondrial transfer mechanisms, it lacks direct visual evidence to confirm the endocytic process. Ideally, direct imaging techniques such as transmission electron microscopy (TEM) to observe mitochondrial translocation and internalization within cells would provide more direct and conclusive evidence. Fourthly, the focus of this study is primarily on endothelial cells in ARDS lung tissue. How MSC-mediated mitochondrial transfer affects overall lung function, inflammatory responses, and long-term repair of lung injury still requires further research for elucidation.

Future research should focus on several key areas: Firstly, an in-depth investigation into the initiating signals of the mitochondrial transfer is needed. This includes elucidating signaling pathways, particularly those that prompt the release of mitochondria from MSCs and the acceptance of mitochondria by MPMECs. Secondly, direct observation of the mitochondrial transfer process will be a key focus of future research. The application of advanced mitochondrial

tracing and imaging techniques to directly monitor mitochondrial translocation will provide critical evidence to support existing hypotheses and enhance our understanding of the dynamics of mitochondrial transfer. Thirdly, exploring the physiological and pathological implications of mitochondrial transfer will help advance its clinical applications. This includes investigating the impact of mitochondrial transfer on cellular functions in various disease models and exploring its potential uses in clinical treatments, particularly in regenerative medicine and tissue repair.

Conclusion

MSCs can transfer mitochondria to ARDS pulmonary endothelial cells, thereby activating the TCA cycle and promoting fatty acid synthesis in endothelial cells. This process further stimulates the release of angiogenic factors and facilitates vascular regeneration. These findings not only provide new

insights into the mechanisms underlying MSC-mediated repair of ARDS lung endothelial injury but also offer novel strategies for utilizing MSCs in the treatment of mitochondrial dysfunction-related diseases.

Ethics approval

Acknowledgements

Disclosure statement

Funding

Data availability statement

The datasets generated and analyzed during the current study are available from the corresponding author on reasonable request.

Author contributions

CRediT: **Jinlong Wang:** Conceptualization, Data curation, Formal analysis, Investigation, Methodology, Visualization, Writing – original draft, Writing – review & editing; **Shanshan Meng:** Conceptualization, Data curation, Funding acquisition, Methodology, Project administration, Writing – review & editing; **Yixuan Chen:** Investigation, Methodology, Resources; **Haofei Wang:** Investigation, Methodology, Resources, Writing – review & editing; **Wenhan Hu:** Formal analysis, Funding acquisition, Investigation, Resources; **Shuai Liu:** Investigation, Methodology, Software, Visualization; **Lili Huang:** Funding acquisition, Investigation, Methodology, Resources; **Jingyuan Xu:** Funding acquisition, Investigation, Methodology, Resources, Visualization; **Qing Li:** Investigation, Methodology, Resources; **Xiaojing Wu:** Conceptualization, Investigation, Methodology; **Wei Huang:** Conceptualization, Investigation, Methodology, Supervision, Writing – review & editing; **Yingzi Huang:** Conceptualization, Funding acquisition, Methodology, Project administration, Supervision, Writing – review & editing

References

[1] Matthay MA, Zemans RL, Zimmerman GA, et al. Acute respiratory distress syndrome. Nat Rev Dis Primers. 2019;5 (1):18.

[2] Bellani G, Laffey JG, Pham T, et al. Epidemiology, patterns of care, and mortality for patients with acute respiratory distress syndrome in intensive care units in 50 countries. Jama. 2016;315 (8):788–800.

[3] Liu L, Yang Y, Gao Z, et al. Practice of diagnosis and management of acute respiratory distress syndrome in mainland China: a cross-sectional study. J Thorac Dis. 2018;10 (9):5394–5404.

[4] Grasselli G, Calfee CS, Camporota L, et al. ESICM guidelines on acute respiratory distress syndrome: definition, phenotyping and respiratory support strategies. Intensive Care Med. 2023;49 (7):727–759.

[5] Hezam K, Wang C, Fu E, et al. Superior protective effects of PGE2 priming mesenchymal stem cells against LPS-induced acute lung injury (ALI) through macrophage immunomodulation. Stem Cell Res Ther. 2023;14 (1):48.

[6] Chen MC, Lai KS, Chien KL, et al. pcMSC modulates immune dysregulation in patients with COVID-19-induced refractory acute lung injury. Front Immunol. 2022;13:871828.

[7] Wang LT, Yen BL, Wang HH, et al. Placental mesenchymal stem cells boost M2 alveolar over M1 bone marrow macrophages via IL-1β in Klebsiella-mediated acute respiratory distress syndrome. Thorax. 2023;78 (5):504–514.

[8] Xu Z, Huang Y, Zhou J, et al. Current status of cell-based therapies for COVID-19: evidence from mesenchymal stromal cells in sepsis and ARDS. Front Immunol. 2021;12:738697.

[9] Beghini DG, Horita SI, Henriques-Pons A. Mesenchymal stem cells in the treatment of COVID-19, a promising future. Cells. 2021;10 (10):2588.

[10] Sharma A, Ahmad S, Ahmad T, et al. Mitochondrial dynamics and mitophagy in lung disorders. Life Sci. 2021;284:119876.

[11] Meyer NJ, Gattinoni L, Calfee CS. Acute respiratory distress syndrome. Lancet. 2021;398 (10300):622–637.

[12] Thompson BT, Chambers RC, Liu KD. Acute respiratory distress syndrome. N Engl J Med. 2017;377 (6):562–572.

[13] Beyer AM, Norwood Toro LE, Hughes WE, et al. Autophagy, TERT, and mitochondrial dysfunction in hyperoxia. Am J Physiol Heart Circ Physiol. 2021;321 (5):H985–H1003.

[14] Liu R, Xu F, Si S, et al. Mitochondrial DNA-induced inflammatory responses and lung injury in thermal injury Rat model: protective effect of epigallocatechin gallate. J Burn Care Res. 2017;38 (5):304–311.

[15] Fuchs B, Sommer N, Dietrich A, et al. Redox signaling and reactive oxygen species in hypoxic pulmonary vasoconstriction. Respir Physiol Neurobiol. 2010;174 (3):282–291.

[16] Spees JL, Olson SD, Whitney MJ, et al. Mitochondrial transfer between cells can rescue aerobic respiration. Proc Natl Acad Sci USA. 2006;103 (5):1283–1288.

[17] Tan AS, Baty JW, Dong LF, et al. Mitochondrial genome acquisition restores respiratory function and tumorigenic potential of cancer cells without mitochondrial DNA. Cell Metab. 2015;21 (1):81–94.

[18] Borcherding N, Brestoff JR. The power and potential of mitochondria transfer. Nature. 2023;623 (7986):283–291.

[19] Dutra Silva J, Su Y, Calfee CS, et al. Mesenchymal stromal cell extracellular vesicles rescue mitochondrial dysfunction and improve barrier integrity in clinically relevant models of ARDS. Eur Respir J. 2021;58 (1):2002978.

[20] Islam MN, Das SR, Emin MT, et al. Mitochondrial transfer from bone-marrow-derived stromal cells to pulmonary alveoli protects against acute lung injury. Nat Med. 2012;18 (5):759–765.

[21] Su Y, Silva JD, Doherty D, et al. Mesenchymal stromal cells-derived extracellular vesicles reprogramme macrophages in ARDS models through the miR-181a-5p-PTEN-pSTAT5-SOCS1 axis. Thorax. 2023;78 (6):617–630.

[22] Morrison TJ, Jackson MV, Cunningham EK, et al. Mesenchymal stromal cells modulate macrophages in clinically relevant lung injury models by extracellular vesicle mitochondrial transfer. Am J Respir Crit Care Med. 2017;196 (10):1275–1286.

[23] Akhter W, Nakhle J, Vaillant L, et al. Transfer of mesenchymal stem cell mitochondria to CD4(+) T cells contributes to repress Th1 differentiation by downregulating T-bet expression. Stem Cell Res Ther. 2023;14 (1):12.

[24] Piekarska K, Urban-Wójciuk Z, Kurkowiak M, et al. Mesenchymal stem cells transfer mitochondria to allogeneic tregs in an HLA-dependent manner improving their immunosuppressive activity. Nat Commun. 2022;13 (1):856.

[25] Liu X, Xia F, Wu X, et al. Isolation of primary mouse pulmonary microvascular endothelial cells and generation of an immortalized cell line to obtain sufficient extracellular vesicles. Front Immunol. 2021;12:759176.

[26] Long G, Gong R, Wang Q, et al. Role of released mitochondrial DNA in acute lung injury. Front Immunol. 2022;13:973089.

[27] Hoang DM, Pham PT, Bach TQ, et al. Stem cell-based therapy for human diseases. Signal Transduct Target Ther. 2022;7 (1):272.

[28] Court AC, Le-Gatt A, Luz-Crawford P, et al. Mitochondrial transfer from MSCs to T cells induces treg differentiation and restricts inflammatory response. EMBO Rep. 2020;21 (2):e48052.

[29] Su Y, Guo H, Liu Q. Effects of mesenchymal stromal cell-derived extracellular vesicles in acute respiratory distress syndrome (ARDS): current understanding and future perspectives. J Leukoc Biol. 2021;110 (1):27–38.

[30] Moradinasab S, Pourbagheri-Sigaroodi A, Zafari P, et al. Mesenchymal stromal/stem cells (MSCs) and MSC-derived extracellular vesicles in COVID-19-induced ARDS: mechanisms of action, research progress, challenges, and opportunities. Int Immunopharmacol. 2021;97:107694.

[31] Zurzolo C. Tunneling nanotubes: reshaping connectivity. Curr Opin Cell Biol. 2021;71:139–147.

[32] Turos-Korgul L, Kolba MD, Chroscicki P, et al. Tunneling nanotubes facilitate intercellular protein transfer and cell networks function. Front Cell Dev Biol. 2022;10:915117.

[33] Ahmad T, Mukherjee S, Pattnaik B, et al. Miro1 regulates intercellular mitochondrial transport & enhances mesenchymal stem cell rescue efficacy. Embo J. 2014;33 (9):994–1010.

[34] Chen J, Zhong J, Wang LL, et al. Mitochondrial transfer in cardiovascular disease: from mechanisms to therapeutic implications. Front Cardiovasc Med. 2021;8:771298.

[35] Chakraborty R, Nonaka T, Hasegawa M, et al. Tunnelling nanotubes between neuronal and microglial cells allow bi-directional transfer of α-synuclein and mitochondria. Cell Death Dis. 2023;14 (5):329.

[36] Alarcon-Martinez L, Villafranca-Baughman D, Quintero H, et al. Interpericyte tunnelling nanotubes regulate neurovascular coupling. Nature. 2020;585 (7823):91–95.

[37] Wick KD, Ware LB, Matthay MA. Acute respiratory distress syndrome. BMJ (Clinical Research ed). 2024;387:e076612.

[38] Zhan B, Shen J. Mitochondria and their potential role in acute lung injury (review). Exp Ther Med. 2022;24 (1):479.

[39] Lu Z, Chang W, Meng S, et al. Mesenchymal stem cells induce dendritic cell immune tolerance via paracrine hepatocyte growth factor to alleviate acute lung injury. Stem Cell Res Ther. 2019;10 (1):372.

[40] Chen J, Li Y, Hao H, et al. Mesenchymal stem cell conditioned medium promotes proliferation and migration of alveolar epithelial cells under septic conditions In vitro via the JNK-P38 signaling pathway. Cell Physiol Biochem. 2015;37 (5):1830–1846.

[41] Currie E, Schulze A, Zechner R, et al. Cellular fatty acid metabolism and cancer. Cell Metab. 2013;18 (2):153–161.

[42] Kalucka J, Bierhansl L, Conchinha NV, et al. Quiescent endothelial cells upregulate fatty acid β-oxidation for vasculoprotection via redox homeostasis. Cell Metab. 2018;28 (6):881–894.e13.

[43] Schoors S, Bruning U, Missiaen R, et al. Fatty acid carbon is essential for dNTP synthesis in endothelial cells. Nature. 2015;520 (7546):192–197.

[44] Levoux J, Prola A, Lafuste P, et al. Platelets facilitate the wound-healing capability of mesenchymal stem cells by mitochondrial transfer and metabolic reprogramming. Cell Metab. 2021;33 (2):283–299.e9.

[45] Li M, van Esch B, Wagenaar GTM, et al. Pro- and anti-inflammatory effects of short chain fatty acids on immune and endothelial cells. Eur J Pharmacol. 2018;831:52–59.

[46] Kang W, Suzuki M, Saito T, et al. Emerging role of TCA cycle-related enzymes in human diseases. Int J Mol Sci. 2021;22 (23):13057.

[47] Martínez-Reyes I, Chandel NS. Mitochondrial TCA cycle metabolites control physiology and disease. Nat Commun. 2020;11 (1):102.